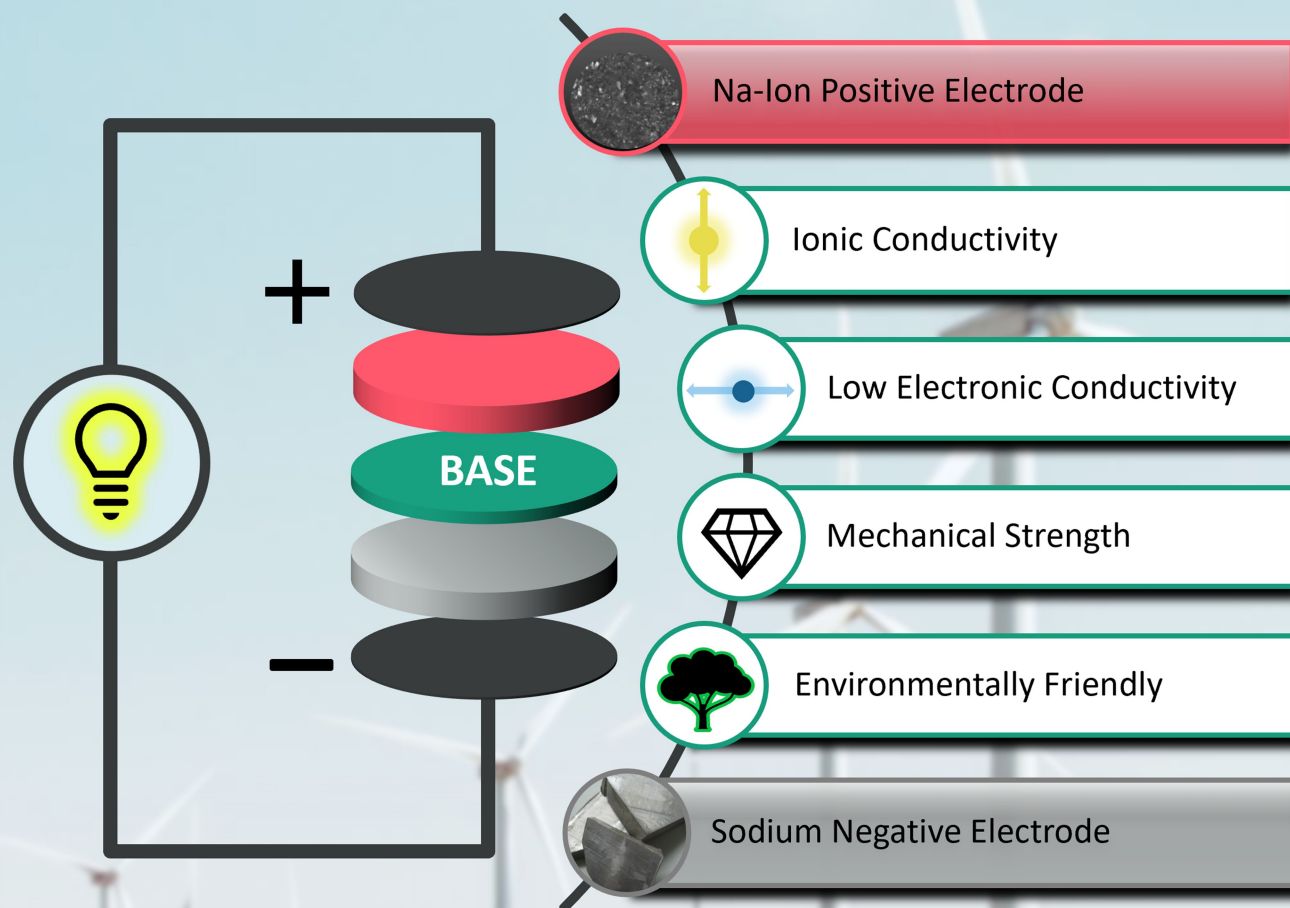VIP *Very Important Paper*

From High- to Low-Temperature: The Revival of Sodium-Beta Alumina for Sodium Solid-State Batteries

Micha P. Fertig,[a, b] Karl Skadell,[b] Matthias Schulz,*[b] Cornelius Dirksen,[a, b] Philipp Adelhelm,[c, d] and Michael Stelter[a, b]

Sodium-based batteries are promising post lithium-ion technologies because sodium offers a specific capacity of 1166 mAh g^{-1} and a potential of -2.71 V vs. the standard hydrogen electrode. The solid electrolyte sodium-beta alumina shows a unique combination of properties because it exhibits high ionic conductivity, as well as mechanical stability and chemical stability against sodium. Pairing a sodium negative electrode and sodium-beta alumina with Na-ion type positive electrodes, therefore, results in a promising solid-state cell concept. This review highlights the opportunities and challenges of using sodium-beta alumina in batteries operating from medium- to low-temperatures (200 °C–20 °C). Firstly, the recent progress in sodium-beta alumina fabrication and doping methods are summarized. We discuss strategies for modifying the interfaces between sodium-beta alumina and both the positive and negative electrodes. Secondly, recent achievements in designing full cells with sodium-beta alumina are summarized and compared. The review concludes with an outlook on future research directions. Overall, this review shows the promising prospects of using sodium-beta alumina for the development of solid-state batteries.

1. Introduction

Due to the increasing competitiveness of renewable energy with fossil energy sources, the transition to sustainable energy supply can be accelerated. Especially the electricity transmission and distribution can be improved by grid energy storage, which would lead to more efficient energy markets and thus, a lower cost of energy.[1] For medium power storage technologies, batteries provide the best solution in terms of life cycle cost of storage and levelized cost of energy, which are metrics to address the economic feasibility.[2] However, high investment costs weaken its position as storage technology, while the shortage of raw materials limits – and environmental pollution caused by battery usage even threatens – the widespread utilization of batteries as a grid storage technology.[3] Meanwhile, current Li-ion battery (LIB) technology approaches its physicochemical limits in energy density.[4] Hence, incremental optimizations of the LIB technology are inevitable (advanced Li-ion) or modifications of Li-ion core components are necessary (post Li-ion) with special respect to material abundance, environmental friendliness, and safety, which are of special importance for grid storage application.[5–8] These post Li-ion technologies promise to solve existing problems (e.g., limited specific energy), while posing new challenges simultaneously. One promising alternative is the substitution of lithium with sodium. Especially for grid storage, where huge amounts of materials are needed, sodium-based batteries with high specific energy based on abundant resources are desirable. Several advantages add up to cell systems when sodium is utilized as the negative electrode, due to the earth's abundance in sodium and therefore low-cost availability[6] while offering a specific capacity of 1166 mAh g^{-1} and a potential of -2.71 V vs. the standard hydrogen electrode. Furthermore, cost reduction might be achieved as it allows the use of aluminum current collectors instead of copper, as sodium does not alloy with aluminum.[6,9–11] On the other hand, sodium-ion batteries (SIBs) still rely on organic, flammable electrolytes which leads to safety challenges comparable to LIBs. Solid-state batteries (SSBs), based on solid electrolytes (SEs), offer a solution to the aforementioned problems and are seen as next-generation batteries, as they promise excellent thermal stability, low flammability, high safety, high specific energy as well as long cycle life.[12–22] Meanwhile, R&D on already commercialized cell systems with sodium as the negative electrode and sodium-beta alumina as solid electrolyte continue. These are the well-known Na/NiCl$_2$- and Na/S-batteries, also known as ZEBRA- and NAS®-batteries, which operate typically between 200 °C and 350 °C and are based on conversion reactions.[23,24] The world-wide capacity of these sodium-beta alumina-based batteries is currently in the GWh range.[25] Applications and challenges of these high-temperature systems and related concepts have been extensively reviewed by different groups in the last decade.[8,10,26–29] The possible use of sodium-beta alumina in gas sensing and thin film transistors has been also discussed.[30] It is even regaining interest as a high-rate sodium-ion electrode.[31] Meanwhile, sodium-beta alumina is increasingly utilized in sodium-based, medium- to low-temperature cell systems due to its unique combination of properties. Research shows, for example, that sodium-beta alumina performs well not only at high but also at low temperatures ($\sigma_{ionic} \approx 5$ mS cm^{-1}).[32] Hence, it may be an option even for room temperature applications. The combination of sodium as the negative electrode, sodium-beta alumina as a solid electrolyte, and Na-ion type positive electrodes results in a promising, medium- to low-temperature solid-state cell concept. Those positive electrodes are already used in Na-ion half and full cells.[33,34] Overview of the research, progress, properties and advantages of positive electrode materials for Na-ion batteries is given elsewhere.[11,35] This review discusses

[a] M. P. Fertig, C. Dirksen, Prof. Dr. M. Stelter
     Center for Energy and Environmental Chemistry Jena (CEEC Jena)
     Friedrich-Schiller-University Jena
     Philosophenweg 7a, 07743 Jena, Germany
[b] M. P. Fertig, Dr. K. Skadell, Dr. M. Schulz, C. Dirksen, Prof. Dr. M. Stelter
     Fraunhofer Institute for Ceramic Technologies and Systems IKTS
     Michael-Faraday-Str. 1, 07629 Hermsdorf, Germany
     E-mail: matthias.schulz@ikts.fraunhofer.de
[c] Prof. Dr. P. Adelhelm
     Department of Chemistry
     Humboldt-University Berlin
     Brook-Taylor-Str. 2, 12489 Berlin, Germany
[d] Prof. Dr. P. Adelhelm
     Joint Research Group Operando Battery Analysis (CE-GOBA)
     Helmholtz-Zentrum Berlin
     Hahn-Meitner-Platz 1, 14109 Berlin, Germany

Batteries & Supercaps

Review
doi.org/10.1002/batt.202100131

Chemistry
Europe

European Chemical
Societies Publishing

key aspects and guidelines for designing sodium-beta alumina and cell concepts based thereon utilizing Na-ion type electrodes, which show insertion reactions. Recent progress in fabricating and doping sodium-beta alumina is presented. The interface design between the solid electrolyte and both the negative and positive electrodes is discussed. The review provides an overview of the progress in using sodium-beta alumina for novel, medium- to low-temperature (200 °C–20 °C) full cells along with a summary on their up-to-date performance values.

## 2. Advantages and Properties of Solid Electrolytes

The development of solid-state cells requires a detailed understanding of solid electrolytes (SE) and their interaction with the electrode materials. This also includes aspects of materials processing, the conduction mechanisms, as well as simulation studies and modeling of the electrolytes and their interfaces.[7,18,21,36–42] The term "solid-state" cell is used in this review because the electrolyte and the positive electrode are solid. Please note that the sodium negative electrode is liquid when the temperature of operation exceeds its melting point. Otherwise, the term "all-solid-state" cell might be used.

The use of solid electrolytes in batteries can provide several benefits compared to using liquid electrolytes. Frequently mentioned advantages associated with using SE are improved safety, higher specific energy, and a wider temperature window.[40,43] These promises, however, still need to be demonstrated on a technological level. Furthermore, chemomechanical issues, which are related to volume changes of the active material in the electrode must be eliminated.[36,39] Combined with poor particle-particle contact, this results in an often insufficient rate capability and cycle life of solid-state cell systems.[20] Recent research for building better Li- and Na-solid-state batteries is summarized in the review from Mauger et al.[44] Utilizing sodium in solid-state batteries and nonaqu-

Micha P. Fertig received his B. Eng. degree in Chemical Engineering from Niederrhein University of Applied Sciences, Krefeld. He received his M.Sc. degree in Chemistry-Energy-Environment from Friedrich-Schiller-University Jena. Now, he is a Ph.D. student with a scholarship of "Graduierten-Akademie Jena" at Fraunhofer Institute for Ceramic Technologies and Systems (IKTS) and focuses on sodium solid-state batteries, sodium-beta alumina, and interface processes.
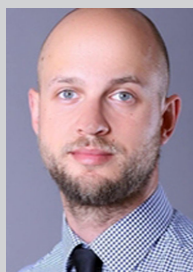
Dr. Karl Skadell received his doctoral degree at the Institute of Chemical Technology in Leipzig for elucidating the key steps in photocatalytic hydrogen evolution. He started working on sodium batteries and hydrogen technologies at the Fraunhofer Institute of Ceramic Technology and Systems (IKTS) in 2017. Dr. Skadell joined the International Electrotechnical Commission's technical committee, which published the standard on high-temperature batteries (IEC 62984–1:2020). Since July 2021, he is responsible for the hydrogen application center of Fraunhofer IKTS close to Erfurt, Germany.

Dr.-Ing. Matthias Schulz is the manager of the workgroup "Stationary Energy Storage Systems" at the Fraunhofer Institute of Ceramic Technology and Systems (IKTS). As a senior scientist, he is responsible for the development of sodium batteries and ceramic based energy conversion and storage technologies. Foci of research are ion conducting ceramics for solid electrolytes, gas separation processes, and applied electrochemistry. Dr. Schulz won the Thuringian award for applied research in 2019 for his work in the field of $Na/NiCl_2$-batteries. He was a Ph.D. student at the Bauhaus University Weimar with a scholarship from the German Federal Foundation for the Environment.

Cornelius Dirksen studied chemistry at the Friedrich-Schiller University Jena. He received his M.Sc. in 2017. Now he pursues his doctoral degree in the field of sodium-beta alumina electrolytes at the workgroup "Stationary Energy Storage Systems" at Fraunhofer Institute of Ceramic Technology and Systems (IKTS). His area of interest focuses on electrolyte production techniques and material optimization.

Prof. Philipp Adelhelm is a professor at Humboldt-University Berlin and is leading a research group on operando battery analysis at the Helmholtz-Zentrum Berlin (HZB). He received his doctoral degree at the Max-Planck-Institute of Colloids and Interfaces in Potsdam. He worked as a postdoc at the Debye Institute of Nanomaterials Science in Utrecht and was a group leader at the Justus-Liebig-University Giessen. From 2015–2019 he was a professor at the Friedrich-Schiller-University Jena. His main interests are on fundamental aspects of rechargeable batteries (Li-ion, Na-ion, sulfur) as well as new cell concepts (solid-state).

Prof. Michael Stelter is a professor for Technical Environmental Chemistry at Friedrich-Schiller-University Jena as well as Deputy Institute Director at Fraunhofer Institute for Ceramic Technologies and Systems (IKTS). He obtained his doctoral degree at TU Chemnitz and worked several years in the industry afterward. In 2005, he started at IKTS. Prof. Stelter's research focuses on appropriate technical-chemical solutions for various environmental issues, e.g., water pollution, and sustainable energy storage technologies.

Batteries & Supercaps

Review
doi.org/10.1002/batt.202100131

Chemistry Europe
European Chemical
Societies Publishing

eous sodium-ion full cells based on solid electrolytes (SEs) were reviewed, too.[17,33,39]

The ideal SE in electrochemical cells must fulfill multiple requirements.

· The SE must be conductive for ions but insulating for electrons when used as a separator. The total ionic conductivity σ_{ionic}, *i.e.*, the bulk and grain boundary ionic conductivity, must be higher than 10^{-4} S cm^{-1} (for composite electrodes 10^{-3} S cm^{-1}). The SE must have negligible electronic conductivity to avoid self-discharge (lower than 10^{-12} S cm^{-1}) and a high transference number (close to 1) for the cation at ambient operating temperature and conditions.[36] High ionic conductivity reduces the area-specific resistance of the electrolyte (ASR$_{electrolyte}$) in combination with a thin SE[22] (compare Section 3.1).

· The SE must have a sufficiently large electrochemical stability window of several volts (*i.e.*, chemical stability against high potential positive electrode as well as a low potential negative electrode) as otherwise additional interface layers are required. Reactions at the electrolyte/electrode interfaces lead to increasing resistance and thus, premature cell death. Thermal as well as mechanical stability are also relevant parameters.[19] Moreover, SEs should inhibit the growth of dendrites on the negative electrode.

· The SE should be non-toxic and non-flammable while offering cost-effective fabrication and easy processing methods.[19]

In the subsequent Sections, sodium-beta alumina shall be compared to above-stated requirements for SEs.

3. Properties of Sodium-Beta Alumina

3.1. Ionic Conductivity and Area-Specific Resistance

A lot of effort was put into the improvement of the ionic conductivity of sodium-beta alumina in the last 50 years. Whittingham and Huggins obtained a conductivity σ of 1.4×10^{-2} S cm^{-1} at 25 °C of small single-crystal beta-alumina

with a reversible electrode in 1971 already.[45] Figure 1A shows that β″-alumina single crystals generally show the highest conductivity followed by β-alumina single crystals and polycrystals. This is due to their different crystal structure (see section 3.2). While β-alumina single crystals follow the Arrhenius-type equation over a wide range of temperature,[45] β″-alumina single crystals don't, probably due to ordering of vacancies at lower temperatures.[46] Due to the change in grain bulk resistance R_b and grain boundary resistance R_{gb}, sodium-beta alumina does not strictly follow the Arrhenius-type equation, either.[47,48] However, single crystals are not practical for application in electrochemical cells. Thus, polycrystalline materials are commonly used in applications. For lithium-stabilized polycrystalline β″-alumina was observed that coarse-grained material (mean grain size around 100 μm) exhibits a higher conductivity than fine-grained material (mean grain size ≤ 2 μm).[49] This indicates that additional grain boundaries impede ion transport. The grain bulk resistance R_b and grain boundary resistance R_{gb} are equal at a specific temperature, while R_{gb} becomes negligible at higher temperatures.[50] Similar results were obtained for polycrystalline sodium-beta alumina.[47,48] Hence, decreasing the grain boundary resistance R_{gb} should be considered for room temperature energy-storage technologies, but seems not essential for high-temperature applications. For the processing of the ceramic, unnecessarily huge grain size is not suggested, because the decrease in resistivity will be negligible compared to mechanical deterioration.[49]

The ionic conductivity σ [Ω^{-1} m^{-1} = S m^{-1}] of solid materials is governed by the ion concentration n [mol m^{-3}], the charge of the mobile ions q [C mol^{-1}] and mobility of the mobile ion carrier μ [m^2 V^{-1} s^{-1}] (Equation (1)):[7,36]

$$\sigma = nq\mu = \left(\frac{\sigma_0}{T}\right) \cdot \exp(-E_a/k_B T) \tag{1}$$

A low activation energy E_a [J] and high temperature T [K] are beneficial for a high mobility (Equation (2)):[36]
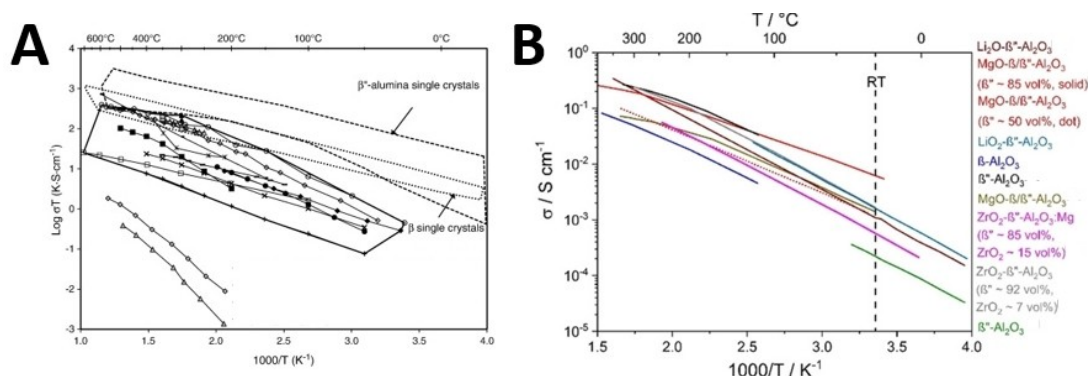

Figure 1. A) Arrhenius-plot of polycrystalline β-, β″- and β / β″-alumina as well as β - and β″-single crystals. For references, please check the original source. Reproduced with permission from Ref. [37]. Copyright (2012) Elsevier B. V. B) Temperature dependence of the total ionic conductivity of different sodium-beta alumina, stabilized with different elements. For references, please check the original source. Reproduced from Ref. [22]. CC BY 4.0, Copyright (2020) The Authors. Published by Wiley-VCH Verlag GmbH & Co. KgaA.

Batteries & Supercaps

Review
doi.org/10.1002/batt.202100131

Chemistry Europe
European Chemical
Societies Publishing

$$\mu \propto \exp(-E_a/k_B T) \tag{2}$$

with k_B [J/K] as the Boltzmann constant. The sodium ion conduction in sodium-beta alumina is attributed to an interstitially mechanism. Here, the ions move between lattice and interstitial sites in the conduction plane.[45] (Sodium) Ion transport and migration mechanisms in solid electrolytes were described in detail in recent reviews.[7,36,39,40] In the past, sodium-beta alumina was mainly utilized in high-temperature batteries with an operating temperature around 250 °C to 350 °C.[51] Hence, ionic conductivities are reported often at this temperature (compare Sections 4.1 and 4.3). However, samples with high ionic conductivities at elevated temperatures point to good conductivity of the ceramic at room temperature (Figure 1B). Thus, values given for elevated temperatures are also relevant for room temperature applications. Recently, Heinz et al. proposed a microstructural model in line with the brick layer model. It gives an explanation to which extent conductivity variations of a BASE sample series with constant composition may be explained by differences in grain size alone. The different grain sizes are due to different sintering regimes. The model helps to identify grain and grain boundary parameters. However, the model can be applied only to dense samples without long dwelling times.[52] Nonetheless, the model is an elegant approach to shed some light on the determining factors for the temperature-dependent conductivity and might be used to predict the temperature dependence of measured conductivity data.

Ionic conductivity is a property of the solid electrolyte material. The area-specific resistance (ASR) [$\Omega\,m^2$] can act as a key performance parameter for the electrolyte (ASR$_{electrolyte}$), but also a whole battery (ASR$_{cell}$). The ASR$_{cell}$ is calculated from the cell resistance R [Ω] and the geometric contact area A between electrode and electrolyte [m^2]. The ASR$_{electrolyte}$ is most often calculated from the conductivity σ [$\Omega^{-1}\,m^{-1}$] and the electrolyte thickness t [m], as shown in Equation (3). Thus, these values normalize resistance to a geometrical area.

$$\mathrm{ASR} = R \cdot A = \frac{t}{\sigma} \tag{3}$$

ASR$_{cell}$ contains resistance contributions from the electrolyte (ASR$_{electrolyte}$) and both the positive and negative electrodes with their respective interfaces (ASR$_{PEI}$ and ASR$_{NEI}$). Equation (3) shows that thin solid electrolytes can compensate for a low ionic conductivity. Several fabrication methods enable sodium-beta alumina with thicknesses around 100 μm already. For instance, thin fabrication of sodium-beta alumina via laser chemical vapor deposition was reported.[53] However, there is a lower limit of electrolyte thickness for brittle or even non-flexible materials, as it is sodium-beta alumina. Mechanical stability of the electrolyte is important to prevent cell failure. Most BASEs show a fracture strength of at least 200 MPa (compare Section 4, Tables 1 and 2). Especially for room temperature solid-state cell systems, high pressure for operation is beneficial. Additional robustness enables the applica-

tion of external pressure more easily, which in turn increases the critical current density (CCD) and thus, specific power of the cell system, as it is shown in Section 5. Beside dendrite growth, also the volume expansion of the electrodes must be considered in sealed cell systems. As Heinz et al. pointed out in their work on pressure management in solid-state batteries, especially planar electrolytes are prone to pressure differences. For example, the pressure difference must not exceed 1.1 bar in a small cell with 3 cm^2 active area, considering a thickness of 200 μm and a fracture strength of 200 MPa.[54] This is important for Na/NiCl$_2$ cells, where the planar cell design experiences increasing interest.[55] However, due to the low volume expansion of insertion electrodes[56] in comparison to, e.g., alloy formation or conversion reactions,[57] the mechanical stress for the BASE during operation is comparably low in cells with Na-ion positive electrodes. No BASE fracture has been reported for this cell system in the literature yet (compare Section 6).

A cell with modified as well as stable interfaces, which are not prone to side reactions, exhibits lower ASR$_{PEI}$ and ASR$_{NEI}$ in comparison to a cell system with identical components with unmodified or unstable interfaces. Hence, the ASR$_{cell}$ highlights aspects of the performance of batteries while including interface processes and interface stability (see Table 3). A "full-cell" ASR (ASR$_{cell}$) can be calculated and used for the comparison of different cell systems. Reducing the ASR$_{cell}$ lowers the overvoltage for any battery application and therefore, increases the energy efficiency. We follow up with two examples. They demonstrate the simple but significant implications of the key parameter ASR for solid-state battery performance. For example, the ASR$_{electrolyte}$ in a Na/NiCl$_2$ cell system equals 0.7 $\Omega\,cm^2$ at 300 °C, when the thickness of the electrolyte component is 1500 μm, as Ma and Tietz stated.[22] To maintain the same ASR$_{electrolyte}$ of 0.7 $\Omega\,cm^2$ at room temperature, the sodium-beta alumina may only be 8 μm thick, since the conductivity decreases with decreasing temperature. To reach an ASR$_{electrolyte}$ of 24 $\Omega\,cm^2$, which is the highest ASR$_{cell}$ of commercial 18650 LIBs[22] when the value is fully determined by the electrolyte material, the moderate room temperature conductivity of sodium-beta alumina of 1×10^{-3} S cm^{-1} is sufficient when the thickness is equal to 240 μm. For comparison, commercial sodium-beta alumina electrolytes exhibit a two- to a four-fold thickness of about 500 μm for tubes and 1000 μm for flat discs.[58,59]

Figure 2(A) illustrates the consequences of the desired ASR$_{electrolyte}$ for the thickness of two sodium-beta alumina electrolytes with different ionic conductivities. As an example, the ionic conductivity of sodium-beta alumina type I (blue) is 5 mS cm^{-1} compared to 1 mS cm^{-1} for type II (orange). Both values are typical values for the room temperature ionic conductivity of sodium-beta alumina (see Tables 1 and 2). To reach an ASR$_{electrolyte}$ of 20 $\Omega\,cm^2$, i.e., a value comparable to ASR$_{cell}$ of commercial LIBs (marked with the red line and dashed area), the sodium-beta alumina (blue) with the higher ionic conductivity might be five times thicker ($t = 1000$ μm, blue arrow) than the other sodium-beta alumina (orange). If an ASR$_{electrolyte}$ of 20 $\Omega\,cm^2$ must be reached with the less conducting sodium-beta alumina (orange), its thickness must

Batteries & Supercaps

Review
doi.org/10.1002/batt.202100131

Chemistry Europe
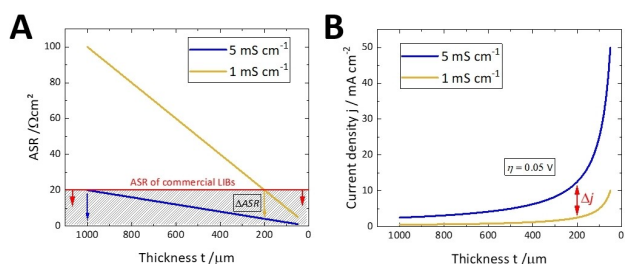European Chemical
Societies Publishing

Figure 2. A) Illustration of the importance of high ionic conductivity of sodium-beta alumina for good performance of a cell system. The ASR$_{cell}$ of commercial LIBs is marked as a red line. An electrolyte with a higher ionic conductivity can be fabricated thicker while reaching the desired ASR$_{electrolyte}$. An electrolyte with a lower ionic conductivity exhibits higher ASR$_{electrolyte}$ compared to an electrolyte with a higher ionic conductivity (orange arrow) when the thickness is the same. B) When the resulting overvoltage shall not exceed, *e.g.*, 0.05 V, the possible current densities are fixed due to the given ASR$_{cell}$. A cell, which utilizes an electrolyte with lower ASR$_{cell}$, can be cycled at higher current densities (red arrow).

(blue) would have been fabricated with only 200 μm thickness, its ASR$_{electrolyte}$ would be as low as 4 Ω cm^2. Figure 2(B) compares the possible current densities of two cells, which utilize the two solid electrolytes (blue and orange) with different ionic conductivities, *i.e.*, different ASRs$_{electrolyte}$. In this example, the Ohmic drop shall not exceed a fixed value of 0.05 V while the ASR$_{cell}$ shall be fully determined by the electrolyte material. The cell, which utilizes the electrolyte with lower ASR (blue), can be cycled at higher current densities (red arrow), despite the equal thickness. Consequently, the cell system utilizing sodium-beta alumina (blue) exhibits a five times higher power density and five times shorter charge/discharge time than the cell system based on sodium-beta alumina (orange).

Hence, ionic conductivity and thickness of sodium-beta alumina as well as interface modifications, which influence the ASR$_{cell}$, are key factors for enabling medium- to low-temperature solid-state cell systems based on sodium-beta alumina. For this reason, attention is aligned on the progress of fabricating the ceramic electrolyte with higher ionic conductivity and/or reduced thickness in the following Sections 4.1, 4.2, and 4.3. Modifications of the interfaces between the negative

be reduced to only 200 μm (orange arrow). This comes at the cost of deteriorating its robustness. If sodium-beta alumina

Table 1. Characteristic values of differently fabricated sodium-beta alumina*.										
Ceramic	δ_{sinter} [°C]	t [min]	β'' [%]	$\rho_{relative}$ [%]	σ [S cm^{-1}]	δ_σ [°C]	E_A [eV]	σ [S cm^{-1}]	δ_σ [°C]	$\sigma_{mechanical}$ [MPa]
α-Al$_2$O$_3$/50 wt% YSZ[88]	1500	240	79	n.a.	1.8×10^{-2}	350	n.a.	*1.3×10^{-6}*	*150*	n.a.
α-Al$_2$O$_3$ / 20 vol%3YSZ[89]	1450	120	**100**	**99**	2.2×10^{-2}	300	0.21	*2.4×10^{-3}*	*72*	350 (B)
Li-BASE[91]	1550	120	96	n.a.	5.6×10^{-2}	300	0.16	*4.7×10^{-3}*	*203*	n.a.
Mg-BASE[90]	1500	360	97	*98*	5.4×10^{-2}	300	**0.19**	*3.5×10^{-2}*	*199*	245 (A)
Mg-BASE[84]	1300	10	86	98	1.8×10^{-1}	350	0.25	*1.7×10^{-3}*	*25*	250 (A)
Mg-BASE[82]	1600	180	93	93	2.4×10^{-1}	350	0.27	*2.0×10^{-3}*	*25*	250 (A)
Mg-BASE[85]	1570	300	96	81	9.7×10^{-2}	350	0.39	*4.5×10^{-5}*	*25*	198 (A)
Li-BASE[76]	1550	30	99	97	3.7×10^{-1}	300	n.a.	n.a.	n.a.	n.a.
Li-BASE[80]	1700	30	84	*93*	2.3×10^{-1}	300	0.17	*1.7×10^{-1}*	*240*	n.a.
Li-BASE[81]	1560	10	96	99	1.2×10^{-1}	300	0.25	*5.5×10^{-4}*	*25*	292 (A)
Mg-BASE[32]	1320	120	84	96	5.4×10^{-3}	25	n.a.	5.4×10^{-3}	25	n.a.

*For conductivities, the highest value, as well as the value at the lowest temperature from the respective publication is given. Bold printed values are estimated from figures in the respective reference. Italic values are calculated from the data given in the respective references. δ_{sinter}: sintering temperature, t: sintering time, β'': β''-phase content, $\rho_{relative}$: relative density, σ: ionic conductivity, δ_σ: Measurement temperature of the ionic conductivity, E_A: activation energy, $\sigma_{mechanical}$: mechanical strength, A: three-point bending method, B: Ring-on-ring method.

Table 2. Characteristic values of differently doped sodium-beta aluminas*.											
Dopant	Amount	δ_{sinter} [°C]	t [min]	β'' [%]	$\rho_{relative}$ [%]	σ [S cm^{-1}]	δ_σ [°C]	E_A [eV]	σ [S cm^{-1}]	δ_σ [°C]	$\sigma_{mechanical}$ [MPa]
Cr$_2$O$_3$[93]	0.15 wt%	1600	10	98	99.1	8.2×10^{-2}	350	0.15	*2.2×10^{-2}*	*97*	253 (A)
TiO$_2$[95]	1.5 wt%	1500	30	94	*97.2*	3.0×10^{-1}	300	n.a.	n.a.	n.a.	175 (Γ)
SnO$_2$[96]	1 mol%	1520	15	99	98.1	5.2×10^{-2}	300	0.35	*1.3×10^{-2}*	*199*	198 (B)
CoO[97]	1 wt%	1600	30	n.a.	98.0	6.1×10^{-2}	300	0.18	*6.3×10^{-2}*	*253*	n.a.
Cr$_2$O$_3$[94]	0.15 wt%	1600	10	94	98.1	1.1×10^{-1}	350	0.16	*2.7×10^{-2}*	*97*	215 (A)
MnO$_2$[77]	0.5 wt%	1600	45	95	98.3	1.7×10^{-1}	350	n.a.	*1.0×10^{-7}*	*25*	n.a.
MnO$_2$[98]	1 wt%	1620	30	98	99.6	1.0×10^{-1}	350	0.21	1.0×10^{-5}	25	n.a.
Ta$_2$O$_5$/ 3YSZ[98]	0.3 wt% / 8 wt%	1620	30	89	97.1	1.1×10^{-1}	350	0.24	4.0×10^{-5}	25	n.a.
Na$_2$O[73]	25 wt%	1450	120	95	97.8	1.2×10^{-2}	350	0.30	*3.5×10^{-3}*	*203*	n.a.
3YSZ[99]	5 vol%	1600	5	n.a.	**97.5**	*1.6×10^{-1}*	300	0.25	*1.4×10^{-1}*	*280*	214 (B)
3YSZ[100]	5 wt%	**1500**	15	94	99.2	7.1×10^{-2}	300	0.27	*4.5×10^{-4}*	*25*	289 (A)
8YSZ[101]	15 wt%	1590	10	89	99.0	1.3×10^{-1}	300	0.23	*4.7×10^{-2}*	*203*	12100 (Δ)

*For conductivities, the highest value, as well as the value at the lowest temperature from the respective publication is given. Boldly printed values are estimated from figures in the respective reference. Italic values are calculated from the data given in the respective references. δ_{sinter}: sintering temperature, t: sintering time, β'': β''-phase content, $\rho_{relative}$: relative density, σ: ionic conductivity, δ_σ: measurement temperature of the ionic conductivity, E_A: activation energy, $\sigma_{mechanical}$: mechanical strength A: three-point bending method, B: Ring-on-ring method, Γ: Ball-on-three-balls method, Δ: Vickers microhardness.

and positive electrode and the solid electrolyte are reported with up-to-date performance values of the respective cells in Sections 5 and 6.

3.2. Crystal Structure

The research of the ceramic sodium-beta alumina started more than a century ago in the year 1916, when Rankin and Merwin investigated the ternary system CaO–Al$_2$O$_3$–MgO and proposed the formula β-Al$_2$O$_3$[60] (β-alumina), which was regarded as an isomorph of Al$_2$O$_3$ at that time.[22] However, in the subsequent years, it was shown that sodium was a key component in the structure, and the influence of sodium ions on the chemical composition and electrical properties was noticed and elucidated in diffraction studies[61–63] and more compounds with slightly different empirical formulas were discovered, *e.g.*, sodium-β′-alumina, which shows great similarity to β-alumina.[64,65] In 1962, Thèry et al. found sodium-β″-alumina while studying the Na$_2$O–Al$_2$O$_3$ system.[66]

It is noteworthy that sodium-β-alumina and sodium-β″-alumina (often simply written as β-alumina and β″-alumina) are not just polymorphs of Al$_2$O$_3$,[67] *i.e.*, the term "alumina" is a misnomer.[68] Often, it is not clear whether the terms stand for the crystal structure or for the solid electrolyte itself. In this review, the terms (sodium-)β-alumina and (sodium-)β″-alumina (Greek letters) are used for the two crystal structures, too, because the terms are commonly used due to historic reasons mentioned above. Sodium-beta alumina and BASE (beta alumina solid electrolyte) are chosen as generic, all-encompassing terms for the fabricated ceramic, which is used as a solid electrolyte. Note, that sodium-beta alumina most often exhibits a mixture of both β-alumina and β″-alumina (compare Table 1 and Table 2) and that they are chemically described as sodium polyaluminates.

The sodium-β-alumina phase and the sodium-β″-alumina phase are two distinguishable layered crystal structures according to the different ratio of sodium to aluminum with the empirical formulas NaAl$_{11}$O$_{17}$ and NaAl$_5$O$_8$, respectively (compare Figure 3).[63,65] Both are examples of a family of complex oxides.[68] The two distinct crystal structures can vary slightly in their composition and thus, often are given as Na$_2$O·nAl$_2$O$_3$ (8 < n < 11 for sodium-β-alumina) and Na$_2$O·mAl$_2$O$_3$ (5 < m < 7 for sodium-β″-alumina).[15,29] Both structures contain excess sodium beside the ideal formula, thus sodium-β-alumina can be also represented as Na$_{1+x}$Al$_{11}$O$_{17+x/2}$ (0.15 < x < 0.3), where excess sodium ions are compensated by oxygen ions. Sodium-β″-alumina is often stabilized by the addition of specific ions, most often Li$^+$ or Mg^{2+} (compare section 4.3), which substitute for Al^{3+}. Additional sodium ions are incorporated in the structure to maintain charge-neutrality so that magnesium-stabilized sodium-β″-alumina can be written as Na$_{1+x}$Mg$_x$Al$_{11-x}$O$_{17}$, where x is normally 0.67.[68] Nowadays, the structure of both phases is fully revealed: It exhibits regions of alternately stacked non-conducting blocks of aluminum oxide separated by loosely packed layers of sodium oxide.[28,30,68] The dense blocks are an arrangement of oxygen ions with aluminum ions sitting on both octahedral and tetrahedral interstices, often referred to as spinel blocks.[27,37] The conduction planes are composed of oxygen and sodium ions, where the latter can move under the applied electric field perpendicular to the c-axis, making the crystals of sodium-beta alumina anisotropic ionic conductors.[69,70] The conduction planes are parallel to the aluminum oxide layers. The unit cell of sodium-β-alumina exhibits a hexagonal crystal structure, containing two spinel blocks and a mirror plane/conduction plane (space group:
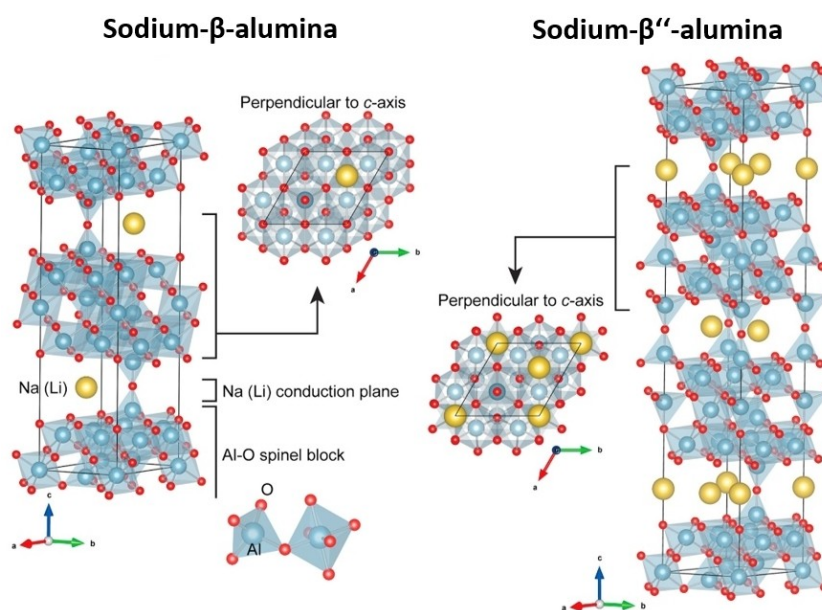

Sodium-β-alumina

Sodium-β″-alumina

Perpendicular to c-axis

Na (Li)

Na (Li) conduction plane

Al-O spinel block

Perpendicular to c-axis

O

Al

Figure 3. Crystal structures of sodium-β-alumina and sodium-β″-alumina. Reproduced with permission from Ref. [71]. Copyright (2016) Elsevier Ltd and Techna Group S.r.l.

Batteries & Supercaps

Review
doi.org/10.1002/batt.202100131

Chemistry Europe
European Chemical
Societies Publishing

$P6_3/mmc$). The sodium-β''-alumina unit cell has a rhombohedral crystal structure (space group: $R\bar{3}m$) and is composed of three spinel blocks with intermediate conduction planes. Mobile sodium ions reside in the conduction planes. Sodium-β''-alumina exhibits a larger fraction of sodium ions as well as a larger unit cell ($a_0 = 0.560$ nm, $c_0 = 3.39$ nm)[64] in comparison to sodium-β-alumina ($a_0 = 0.559$ nm, $c_0 = 2.261$ nm).[61,63] Both factors have a positive impact on the ionic conductivity of sodium-β''-alumina.[70] The lattice parameters vary slightly depending on the reference.[30,64] Hence, sodium-β''-alumina is the preferred phase for sodium-beta alumina used in cell systems and a high sodium-β''-alumina phase purity is desired for fabrication of the solid electrolyte.

4. Recent Progress in Fabrication and Doping Methods of Sodium-Beta Alumina

Generally, multiple methods exist for synthesizing sodium-beta alumina powders, *e.g.*, sol-gel processes or solid-state reactions. For solid-state reaction, α-Al_2O_3 is mixed with appropriate amounts of sodium salts as well as Li- and/or Mg-salts.[28] Note that several alumina precursors can be used, but it was found that the sodium-β''-alumina content is strongly dependent on the alumina source.[72,73] After mixing, several ball milling and calcination steps, followed by final sintering treatment are necessary. Detrimental is the high sintering temperature of around 1600 °C at the solid-state reaction (*i.e.*, sodium loss and grain growth), moisture sensitivity due to $NaAlO_2$ residue along the grain boundaries and the resulting two-phase mixture of β/β''-alumina, where β-alumina's presence lowers the ionic conductivity.[28] Slip casting, extrusion,[59,74] and isostatic pressing are methods for forming the solid electrolyte.[24] Newer methods include tape casting and chemical vapor deposition (CVD). Tape casting results in large and planar BASE membranes,[75] and CVD results in thin BASE membranes.[53] For details of fabrication of sodium-beta alumina, it is recommended to consider reviews focusing on the synthesis and fabrication methods, *e.g.*, from Lu et al.[27,28] The research shows that properties like microstructure, porosity, relative density, β''-phase, activation energy, ionic conductivity, and mechanical strength of sodium-beta alumina are heavily influenced by the production process (*i.e.*, fabrication/material processing of sodium-beta alumina and sintering methods at different sintering temperatures and sintering times) and doping. Both have been studied over decades. Nonetheless, the focus is still dedicated to the improvement of fabrication methods, both conventional solid-state fabrication and methods besides conventional solid-state fabrication as well as doping. The results are covered in Sections 4.1, 4.2, and 4.3, respectively. Only the latest literature of the last three years (2018–2021) is presented to give the reader an up-to-date overview of the topic. In the following schemes and tables, the results of several publications are shown and listed. Please note that only the results of the material with the highest ionic conductivity with the respective measurement temperature are shown in Tables 1

and 2, even if multiple materials or preparations methods were investigated in the respective publications. Furthermore, literature proposes different calculation methods for sodium-β''-alumina fractions.[76] Thus, the comparison of sodium-β''-alumina fractions from various publications can be misleading.

4.1. Influence of Conventional Solid-State Fabrication Methods on the Properties of Sodium-Beta Alumina

A common modification of the solid-state method is the double-zeta method (see Figure 4(A)). Here, the stabilizers are sodium aluminate and lithium aluminate. The method tries to achieve a more homogeneous Li^+ distribution in the green compact. Here, β''-alumina conversion shall be enhanced in comparison to the conventional solid-state method.[77,78] Lee et al. performed both processes in a single synthesizing-cum-sintering process, combining the synthesizing and firing steps. The synthesis temperature of 1400 °C with sintering at 1600 °C leads to a high relative density, which was ascribed to the pre-consolidation effects during the synthesis process.[77]

Furthermore, the sintering conditions and liquid phase formation temperature are of utmost importance for the microstructure and ionic conductivity of samples prepared by solid-state synthesis. This was demonstrated in a comprehensive study from Bay et al. for Li-stabilized sodium-beta alumina, prepared from identical starting powders while varying the fabrication conditions.[76] The relative sintered density of the final ceramics was independent of the green densities. This result points towards a liquid phase formation at a eutectic temperature of 1503 °C. Surprisingly, the composition and β''-phase content of sodium-beta alumina, prepared from identical green bodies, did not depend on the sintering profiles (Figure 4(B)). The profiles were varied in maximum sintering temperature and dwell times. However, a sintering temperature above 1500 °C had a huge impact on the microstructure. It led to an abrupt increase of relative densities, which was again related to the formation of the liquid phase (compare Figure 4(C)). Above a temperature of 1600 °C the density decreased due to Na_2O evaporation. Grain growth was observed with increasing temperature and dwelling times, resulting in ionic conductivities from 4×10^{-2} S cm^{-1} up to 3.7×10^{-1} S cm^{-1} at 300 °C (see Table 1). Once more, an abrupt increase is observed at the formation temperature of the liquid phase at 1500 °C, resulting in the densification of the sample. However, the sample with the highest conductivity featured grains larger than 100 μm and pores larger than 20 μm. The sample is therefore unsuitable for battery application because the grains and pores significantly reduce the mechanical stability. Unfortunately, fracture or bending strengths were not given for these samples.
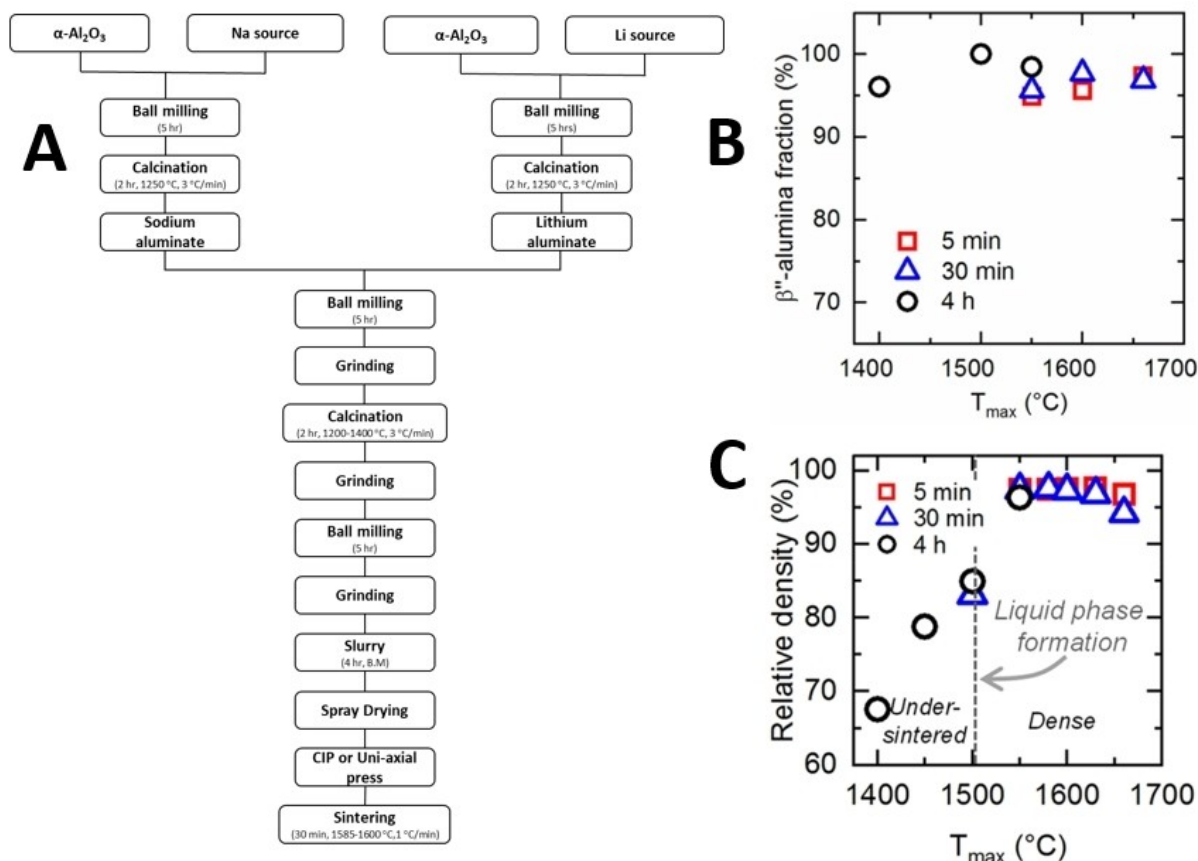
Figure 4. A) Schematic of the double-zeta method. Redrawn after Ref. [77]. B) β''-alumina fractions of ceramics sintered at different temperatures and dwelling times. C) Impact of sintering temperature on the relative density. For temperatures $> 1500\,°C$, the ceramics are dense. Reproduced with permission from Ref. [76]. Copyright (2019) American Chemical Society.

4.2. Influence of Fabrication Methods Beside Conventional Solid-State Fabrication on the Properties of Sodium-Beta Alumina

Conventional solid-state synthesis relates to high sintering temperatures and limitations of reducing the thickness. Loss of sodium is observed above 1300 °C, which results in compositional and structural changes in unprotected ceramics and exaggerated grain growth. Therefore, encapsulation[79] or mitigating high temperatures is beneficial to obtain the desired composition. Undesired, rapid grain growth is prevented when sintering is performed quite quickly. To prevent high sintering temperatures and to avoid challenges connected to conventional solid-state fabrication, alternative fabrications methods are explored.

The simple and versatile sol-gel route based on the Pechini method resulted in Li-stabilized sodium-beta alumina with high ionic conductivity but suffers from the high sintering temperature of 1700 °C.[80] For optimization of homogeneity of sodium-beta alumina, non-aqueous gel casting seems to be an appropriate method. SEM images of gel casted samples showed a homogeneous and densified microstructure (Figure 5(B)).[81] Gel casting is a more complex multi-step fabrication method due to an increased number of involved steps and

chemicals. If the fabrication results in thinner electrolytes it could be worthwhile because it would have a huge influence on the $ASR_{electrolyte}$ (compare Section 2). However, no thicknesses were given in the aforementioned publication.

Low sintering temperatures of 1300 °C were achieved with spark plasma sintering, which is an attractive method[83] due to its faster heating rate and shorter sintering time. The grains in the sintered samples partially inherited the microstructure of their precursors (i.e., the grains grew preferentially in a specific direction) as indicated from XRD measurements.[84] Preparation of the Mg-stabilized alumina powder from one-dimensional rod-shaped boehmite by ice templating and freeze-drying enabled spark plasma sintering at even lower temperatures of only 1100 °C. Here, the slurry is freeze-dried and then sublimated into vapor in a vacuum state. Again, it was indicated that the microstructure of the sodium-beta alumina was inherited from the precursor, which was also observed from samples fabricated by solid-state reaction,[85] resulting in a "brick-bridge-mortar" crystal structure (Figure 5(A)).[82] The inheritance is interesting due to the anisotropic character of sodium-beta alumina but did not result in higher ionic conductivities yet (compare Table 1).

A promising approach was the fabrication of only 50 μm thick sodium-beta alumina via thin-film technique with one of
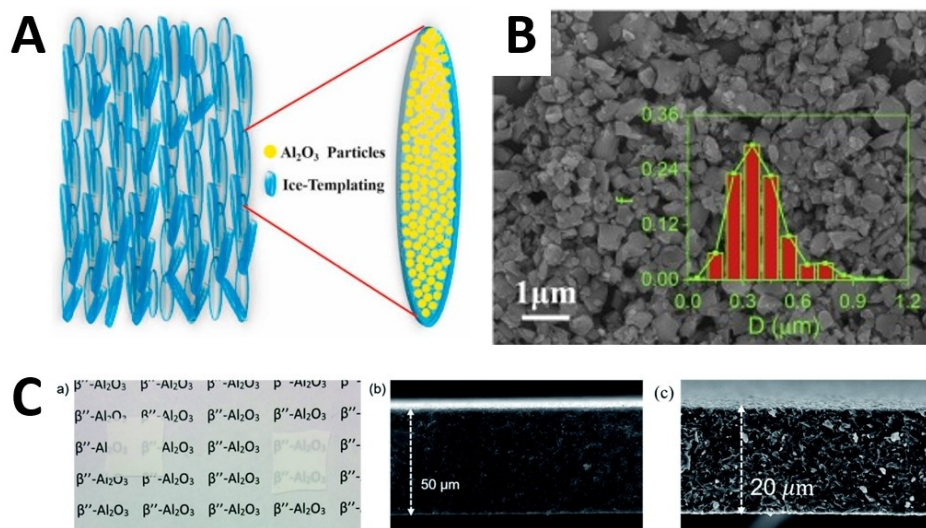
Batteries & Supercaps

Review
doi.org/10.1002/batt.202100131

Chemistry
Europe
European Chemical
Societies Publishing

Figure 5. A) Schematic of the particle orientation induced by ice template. Reproduced with permission from Ref. [82]. Copyright (2021) Elsevier Ltd and Techna Group S.r.l. B) SEM of the particles in the mixture, with the particle size distribution curve shown in the inset. Reproduced with permission from Ref. [81]. Copyright (2020) Elsevier Ltd. C-a) Optical image of sodium-beta alumina with an area of roughly 2×2 cm^2, C-b) SEM fracture surface image of sodium-beta alumina (50 μm thick), C-c) fracture surface of a 20 μm thick film. Reproduced with permission from Ref. [32]. Copyright (2018) the Royal Society of Chemistry.

the lowest reported sintering temperatures of only 1320 °C (Figure 5C). A 50% sodium excess was selected, because it was assumed that the loss rate is much faster in thin samples, compared to thick pellets. The addition of flame synthesized TiO$_2$ and ZrO$_2$ nanopowders (28 nm and 32 nm) aided sintering and successfully inhibited grain growth. The thin films were translucent and offered a room temperature ionic conductivity of 5.4 mS cm^{-1}.[32] Note that the resulting ASR$_{electrolyte}$ is below 1 Ω cm^2 and thus, comparable with already commercialized LIBs (see Section 2). Hence, novel cell designs with flat geometries and room temperature operations may be realized.

Another synthesis method besides conventional solid-state synthesis is the vapor phase synthesis.[86] For vapor phase synthesis, a mixture of Al$_2$O$_3$ and Y$_2$O$_3$-partially stabilized zirconia powder (YSZ) is pressed into discs and then heat treated.[28] ZrO$_2$ is most often stabilized with 3 or 8 mol% Y$_2$O$_3$, resulting in 3YSZ and 8YSZ, respectively. The discs are converted to sodium-beta alumina by placement in a packing powder (i.e., NaAlO$_2$, LiAlO$_2$, and α-Al$_2$O$_3$).[87] The Na$_2$O sublimates onto the ceramic during subsequent heat treatment, which is converted to sodium-beta alumina in a solid-state reaction. YSZ provides oxygen paths for ion diffusion during the vapor phase conversion of α-Al$_2$O$_3$ to sodium-beta alumina (compare Figure 6). In contrary to the conventional process, no stabilizers (Li$^+$, Mg^{2+}) for the β″-phase are needed due to lower conversion temperature. Furthermore, the grain size remains constant after conversion.[28] Vapor phase synthesis was chosen from different groups for the fabrication of sodium-beta alumina.[88–91] Nano-η-alumina can be used to synthesize β″-alumina by a vapor phase process[91] and γ-Al$_2$O$_3$ instead of α-Al$_2$O$_3$ can be used for synthesis to overcome a large amount of β″-alumina powder since γ-Al$_2$O$_3$ and sodium-β″-alumina exhibit similar structures. The powder is needed for vapor

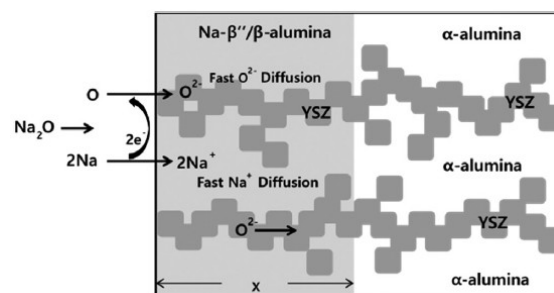**Figure 6.** Illustration of the conversion process from α-alumina/YSZ composite to Na$^+$-β/β″-alumina/YSZ composite electrolyte by vapor phase conversion. Reproduced with permission from Ref. [88]. Copyright (2019) Elsevier.

phase conversion.[90] Lee et al. reported a steady increase in ionic conductivity with increasing mass fraction up to 50% YSZ.[88] Ligon et al. found a significantly lower ionic conductivity when comparing samples fabricated via vapor phase conversion (20% 3YSZ) with conventionally sintered samples without 3YSZ at 300 °C (0.022 S cm^{-1} vs. 0.18 S cm^{-1}), but an increase in strength up to 350 MPa. Interestingly, samples prepared with a higher amount of yttria (8YSZ) performed worse than their counterparts with less yttria (3YSZ), both fabricated via vapor phase synthesis. Hence, 8YSZ does not beneficially assist the oxygen diffusion for phase conversion, despite its higher oxygen diffusion value/bulk oxygen conductivity. The activation energy was only 0.21 eV for the vapor phase sample.[89] This fact and the high flexural strength make the vapor phase conversion a consideration for fabricating sodium-beta alumina for room temperature applications (for the importance of mechanical strength for room temperature application compare section 5).

These examples show that the fabrication methods, the sintering regimes, and the features of the starting powders have a huge impact on the properties of the ceramic electrolyte. However, most of the fabrication methods do not significantly improve the conductivity of sodium-beta alumina (see Table 1). Scalable methods for the fabrication of thin electrolytes are advantageous and promising. Thin electrolytes diminish the ASR$_{electrolyte}$, which is beneficial for cell systems.

4.3. Influence of Doping on the Properties of Sodium-Beta Alumina

The stabilities of both the sodium-β-alumina as well as sodium-β''-alumina phase is dependent upon dopants, which can alter the properties of the alumina system. Sodium-β''-alumina is the preferred phase in cell systems due to its higher conductivity. Its high temperature stability is improved by adding monovalent (Li$^+$, regarded as the most effective dopant), divalent (Cd^{2+}, Co^{2+}, Cu^{2+}, Mg^{2+}, Mn^{2+}, Ni^{2+}, Zn^{2+}) or tetravalent (Ti^{4+}) cations.[30,70] Those cations occupy tetrahedral or octahedral sites of the spinel block (ionic radius < 0.097 nm, Boilot and Thery's theory).[92] Furthermore, replacing Al^{3+} in the spinel blocks by a cation with a lower charge results in a charge imbalance and an alteration of the concentration of mobile Na$^+$ in the conduction plane. Most often, this is done by adding Mg^{2+}.[28] The charge imbalance is overcome by either incorporating a larger number of Na$^+$ or a lower number of oxygen interstitials in the conduction plane, or a lower number of aluminum vacancies in the spinel layer.[70] Modeling and simulations of the influence of dopants on ionic transport mechanism were reviewed by Åvall et al.[38] Table 2 shows the properties of different sodium-beta alumina doped with Cr$_2$O$_3$,[93,94] TiO$_2$,[95] SnO$_2$,[96] CoO,[97] MnO$_2$,[77,98] Ta$_2$O$_5$,[98] and Na$_2$O.[73] All doped samples exhibited higher ionic conductivities in comparison with the undoped specimens. 0.15 wt% Cr$_2$O$_3$ also enhanced the content of the β''-phase, the relative density, and the bending strength, while additional chromium elements would accumulate in the grain boundary and hinder the β''-phase formation.[93] Also, the optimal doping amount of 0.15 wt% Cr$_2$O$_3$ was confirmed for the synthesis via a citrate-nitrate combustion method with similar performance values.[94] An improved β''-phase fraction was found for doping a sample with 0.5 wt% MnO$_2$ for a synthesizing-cum-sintering fabrication, too.[77] In a follow-up study, Lee et al. identified the 1 wt% MnO$_2$ sample as the one with the highest conductivity. Here, also a Ta$_2$O$_5$-doped sample was prepared with 8 wt% 3YSZ, where only 0.4 wt% of Ta$_2$O$_5$ already led to a secondary phase.[98]

Another advantage for a doped sample is the lowered sintering temperature without losing stability nor conductivity, as it was observed for 1.0 wt% TiO$_2$[95] and 1 mol% SnO$_2$.[96] However, mechanical deterioration was found for TiO$_2$ due to larger grain size, while SnO$_2$ improved the densification behavior and fracture strength. A more densified microstructure was observed for samples doped with 1 wt% CoO, while excess doping with only 1.25 wt% CoO already deteriorated

the sample density and thus, the ionic conductivity.[97] Hence, also high conducting sodium-beta alumina samples can be further improved by adding appropriate amounts of dopants.

Last, the degree of densification can be altered with additives, mainly MgO[102] and ZrO$_2$, impacting the resistivity and strength.[70] As for the vapor phase conversion, ZrO$_2$ is most often stabilized with 3 or 8 mol% Y$_2$O$_3$, resulting in 3YSZ and 8YSZ. In comparison to other dopants, it does not alter the crystal structure, but accumulates in the grain boundary and delays grain growth.[101] ZrO$_2$ enhances not only the strength up to 100% but also increases resistivity towards humidity. However, it also decreases ionic conductivity due to accumulation on the grain boundary, increasing the grain boundary resistance and percolation path.[103] A reduced ionic conductivity in comparison to the undoped sample was observed for samples, which were fabricated with a 3YSZ composite beta alumina precursor. Li et al. found that the addition of 3YSZ on the alumina particle surface hindered the transport of matter during phase formation, resulting in an increased diffusion distance of the substances. Hence, for samples with 3YSZ addition, a higher temperature or longer times are needed for β/β''-alumina phase transformation. Nonetheless, the uniform distribution of nano ZrO$_2$ via spray drying had a beneficial effect on the microstructure and densification, resulting in a higher Weibull's modulus and higher characteristic strength. It was detrimental to the ionic conductivity due to the increase of grain boundary resistance.[100] Bay et al. showed that the 3YSZ addition decreased the liquid phase formation temperature by 60 °C due to its impact on the grain boundary composition. 5 vol% 3YSZ decreased the ionic conductivity while increasing the flexural strength.[99] Unfortunately, Li et al. did not investigate the liquid phase formation temperature in the study, where they added 15 wt% 8YSZ to the specimen. The 15 wt% 8YSZ addition supported the densification and β- to β''-phase transformation at low temperature during sintering, which was described as pore control process. It was suggested to sinter the specimens at higher temperatures and short dwell times for high β''-phase fraction and high relative density. Nearly the same activation energies were obtained for the doped and undoped samples, indicating that YSZ addition does not hinder ion migration in the lattice.[101] This result is in line with the study from Bay et al. for different volume percentages of 3YSZ in the specimens, in which the activation energy was constant for samples with and without 3YSZ in a temperature range from 280 °C to 320 °C.[99] A study from Li et al. with 5 wt% 3YSZ specimens contradicted those findings. It indicated that 3YSZ was able to introduce a sodium ion transport barrier. Here, they took a larger temperature range into account.[100] Generally, the vapor phase converted sodium-beta alumina with YSZ exhibited significantly lower activation energies in comparison to their directly sintered specimens with YSZ (0.20 eV vs. 0.30 eV) due to the smaller average grain size, as mentioned in Section 4.1.[89] Since grain boundary resistances R_{gb} become more prominent at lower temperatures, the addition of YSZ to fabricate sodium-beta alumina should be considered carefully for cell concepts operating at room temperature.

Batteries & Supercaps

Review
doi.org/10.1002/batt.202100131

Chemistry Europe
European Chemical
Societies Publishing

4.4. Chemical and Electrochemical Stability

Insufficient chemical stability of the solid electrolyte induces interfacial degradation. The degraded interfaces increase the resistance and the total overvoltage. Therefore, interface engineering of the negative and positive electrodes is necessary (see Sections 5 and 6). Hence, electrolytes with high macroscopic conductivity can still exhibit high impedances when no favorable compatibility with the electrodes is manifested.[7] But to supersede Li-ion technology, novel cell systems must utilize a sodium negative electrode, which can significantly increase the specific energy.[12] Challenges arise from the low Coulomb efficiencies and thus, limited cycle life. This is due to side reactions that lead to loss of active material and corrosion of the solid electrolyte. A prolonged cycle life requires further understanding of interfacial processes and chemistry.[104] Luckily for cell systems based on sodium-beta alumina, this solid electrolyte shows excellent stability against sodium metal.

The interface stability of sodium-beta alumina was addressed in density functional theory calculations, showing remarkable stability against reduction by sodium metal. For $NaAl_{11}O_{17}$, instability below 0.14 V vs. Na/Na$^+$ was calculated, decomposing the β-alumina phase to $NaAlO_2 + Al$. Luckily, the reaction energy for the compositions is less than 25 meV atom^{-1}, and stabilization is likely due to structural disorder. The oxidation occurs at approximately 4 V vs. Na/Na$^+$ (Figure 7A). Furthermore, the ceramic shows resilience to variations in cathode chemistry.[41]

The stability was demonstrated experimentally for the ceramic solid electrolyte, too, on which sodium metal was pressed onto both sides of the ceramic pellet. The stability was investigated with impedance and polarization measurements as well as in situ X-ray photoemission spectroscopy (XPS). The Nyquist plot showed no change over time, while the cyclic voltammetry indicated no change in polarization resistance during the measurement (Figure 7B). No decomposition products were observed with in situ XPS-measurements (Figure 7C), which corroborates the interfacial stability of sodium-beta alumina against sodium metal. This makes sodium-beta alumina "the material of choice" for cell systems with protected sodium metal negative electrodes, as it shows excellent stability, as Wenzel et al. stated.

Additionally, an electronic conductivity σ_e of 6×10^{-12} S cm^{-1} was determined by the use of blocking gold electrodes via dc measurement.[105] This electronic conductivity is consistent with other reported values, e.g., $\sigma_e = 7 \times 10^{-11}$ S cm^{-1} reported at room temperature, following Arrhenius behavior with an activation energy of 0.42 eV.[106,107] Hence, sodium-beta alumina clearly fulfills the requirements for chemical stability against sodium as well as electronic insulation to prevent self-discharge stated in Section 2.

Ansell summarized research for decomposition at high and low potentials.[108] Anodic decomposition of sodium-beta alumina was no concern in electrochemical cell tests, which will be presented in Section 6, where cells were cycled to an upper voltage up to 4.5 V vs. Na/Na$^+$.

Hence, sodium-beta alumina shows chemical stability against sodium and electrochemical stability. However, expos-
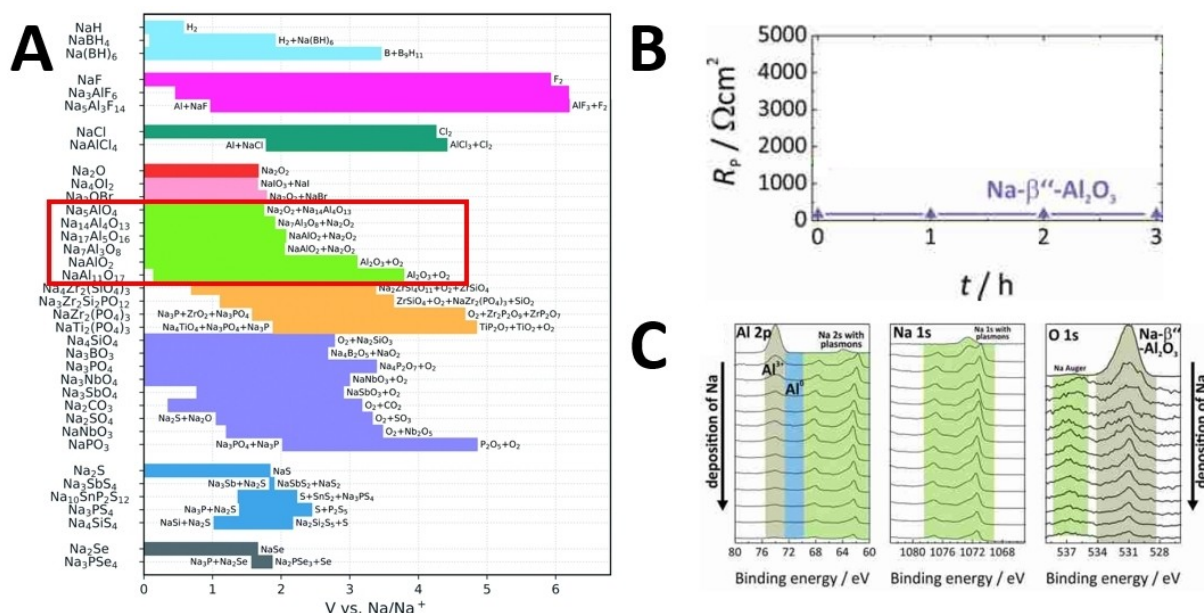

Figure 7. A) Calculated electrochemical stability windows of different sodium solid electrolytes. The different oxides are distinguished by different color. The sodium aluminates are highlighted with the red rectangle. Reproduced from Ref. [41]. CC BY 3.0, Copyright (2019) The authors, published by The Royal Society of Chemistry. B) No change in the polarization resistance corroborates the interfacial stability of sodium-beta alumina against sodium metal. Reproduced with permission from Ref. [105]. Copyright (2016) American Chemical Society. C) Results of the in situ XPS measurements, where Na was sequentially deposited on sodium-beta alumina. Here, no changes in the chemical states of O and Al can be observed. This confirms the interfacial stability of sodium-beta alumina against sodium metal. Reproduced with permission from Ref. [105]. Copyright (2016) American Chemical Society.

Batteries & Supercaps

Review
doi.org/10.1002/batt.202100131

**Chemistry
Europe**
European Chemical
Societies Publishing

ing the ceramic to water or water vapor leads to the occlusion of water and diffusion of hydronium ions into the crystal lattice. The occlusion is a fast process, happening in a time frame of hours.[109] A surface layer of several micrometer forms.[110] Occlusion and diffusion lead to ion exchange in the conducting plane. The latter process is not finished within days.[109,111] β''-alumina is more prone to water intake than β-alumina. Those two effects increase the resistivity of the SE significantly.[109,112,113] Therefore, researchers should limit the exposure time of sodium-beta alumina to moisture to a minimum and consider heat treatment[112] before usage.

5. Negative Electrode Interface Modifications and Dendrite Growth

The preceding sections highlighted the structure of sodium-beta alumina, as well as its properties, e.g., ionic conductivity and mechanical strength, and how they are altered by fabrication methods and dopants. The sections highlighted that the solid electrolyte (SE) shows fine chemical and electro-chemical stability. However, chemical stability does not inevitably induce low interfacial resistance, which is correlated to surface chemistry and wettability.[114] As it can be seen on the number of reviews regarding interface modifications for different SEs,[15,16,18–21] a paradigm shift has happened: The performance of solid-state cell systems is not limited by the ionic conductivity of the solid electrolyte (SE) anymore but by the insufficient interface contact between the rigid SE with both of its adjacent electrodes. Intimate contact for sufficient charge transfer over the electrode/electrolyte interfaces, in tandem with mechanical and structural stability are key requirements for a well-performing cell. Hence, modifications methods of SEs and the understanding of interfacial stability of SEs for novel cell systems are of huge importance.[13,115] Furthermore, high power density could be hindered due to potential dendrite growth. Both aspects apply for cell systems based on sodium-beta alumina, which are most often neglected when considering SEs despite the progress. Surface treatment and modification methods are needed, especially for cell systems operating at medium to room temperature, where sodium wetting is difficult to maintain. A reasonable sodium wetting, i.e., an intimate interface contact between the sodium negative electrode and sodium-beta alumina, results in low polarization, and thus, in enhanced electrochemical cell performance and prolonged cell life. Reasonable sodium wetting is achieved for wetting angles $\theta < 90°$ (see Figure 8A).[116]

Already in 1985, the modification of the sodium-beta alumina surface with Pb/PbO was proposed by Sudworth and Tilley, followed by other modifications methods, e.g., Ni nano-wires, Bi and Sn.[121] Chang et al. treated the sodium-beta alumina surface with lead acetate trihydrate (LAT). Subsequent heating to 400 °C resulted in the formation of spherical lead particles on the surface with minor byproducts of Pb(II). The wetting configuration was proposed to be a "sunny-side-up drop", differing from the previously proposed Young-Dupré

relation for smooth surfaces. The application of sodium on this Pb-decorated sodium-beta alumina resulted in a significantly smaller wetting angle of sodium on the sodium-beta alumina surface. It increased the performance of the Na/NiCl$_2$ test cell.[116] Li et al. extended the heat treatment temperature with LAT to 550 °C. It resulted in a wetting angle close to 0° at 120 °C, i.e., perfect sodium wetting. The improved wetting lowered the Na/S cell's interfacial resistance, enhanced specific capacity, and improved the long-term cyclability of the cell system.[122] Na wetting engineering was done by Jin et al. on another Na/NiCl$_2$ cell. Here, bismuth deposition on sodium-beta alumina effectively eliminated moisture and enhanced the wetting of liquid sodium, resulting in a decreased Ohmic resistance (see Figure 8B).[117] This makes the application of bismuth a viable coating especially for low-temperature Na/NiCl$_2$ cells and therefore, also novel cell systems with sodium negative electrodes working at low-temperature. Both up-to-date results, published in the last three years (2018–2021), show clearly that modification methods enhance the performance of cell systems with a sodium negative electrode. However, it is questionable, whether the application of high cost or toxic metal coatings can be a practical solution for sustainable energy storage. Therefore, several other approaches were investigated in the last three years. For example, Lu et al. designed a Na$_x$MoS$_2$–C–BASE triple junction interface by dispersing MoS$_2$ and carbon in molten sodium. The composite had a small wetting angle of only 45° on BASE. It showed a significantly reduced ASR$_{NEI}$ in symmetrical solid-state cells and enhanced the performance of a Na/S test cell.[123] Another possible approach was the introduction of cotton-cloth-derived disordered carbon tubes (DCTs) on the surface of sodium-beta alumina. The DCTs were prepared by carbonizing the cotton cloth under an argon atmosphere at 1100 °C. Afterward, a slurry of NMP, PVDF, and DCT powder was cast on the sodium-beta alumina. The carbon tubes provided enough space for sodium deposition and reduced the contact angle of molten sodium on the sodium-beta alumina surface to 30° at 300 °C. The resistance dropped from 750 Ω cm^{-2} (sic!) in a Na/BASE/Na cell to 150 Ω cm^{-2} (sic!) in a Na/DCT-BASE/Na symmetrical cell. Our calculation with a diameter of 12 mm for the symmetrical cell gives an ASR$_{cell}$-drop from 958 Ω cm^2 to 192 Ω cm^2. Note that the figure in the original source shows a drop from roughly 1600 Ω cm^2 to 300 Ω cm^2. Nonetheless, the interface impedance was successfully reduced by this low-cost strategy.[124] A porous carbon coating, consisting of carbon black particles and sodium hexametaphosphate dispersed in an isopropanol-water solution (see Figure 8C), successfully reduced the ASR$_{cell}$ of a Na/BASE/Na cell to only 1.3 Ω cm^2 at an operating temperature of 250 °C. The ASR$_{electrolyte}$ contributed about 0.8 Ω cm^2.[118] The coating provided electrons and acted as a reservoir for liquid sodium while wetting the sodiophilic sodium-beta alumina surface. This ASR$_{electrolyte}$ is suitable for practical application (compare Section 2), presupposed the positive electrode in a full cell does not increase the ASR$_{cell}$ considerably. Carbonaceous additives also played a role in a more sophisticated approach for reducing the ASR$_{electrolyte}$, wherein a bi-layer sodium-beta alumina was fabricated. Two different slurries
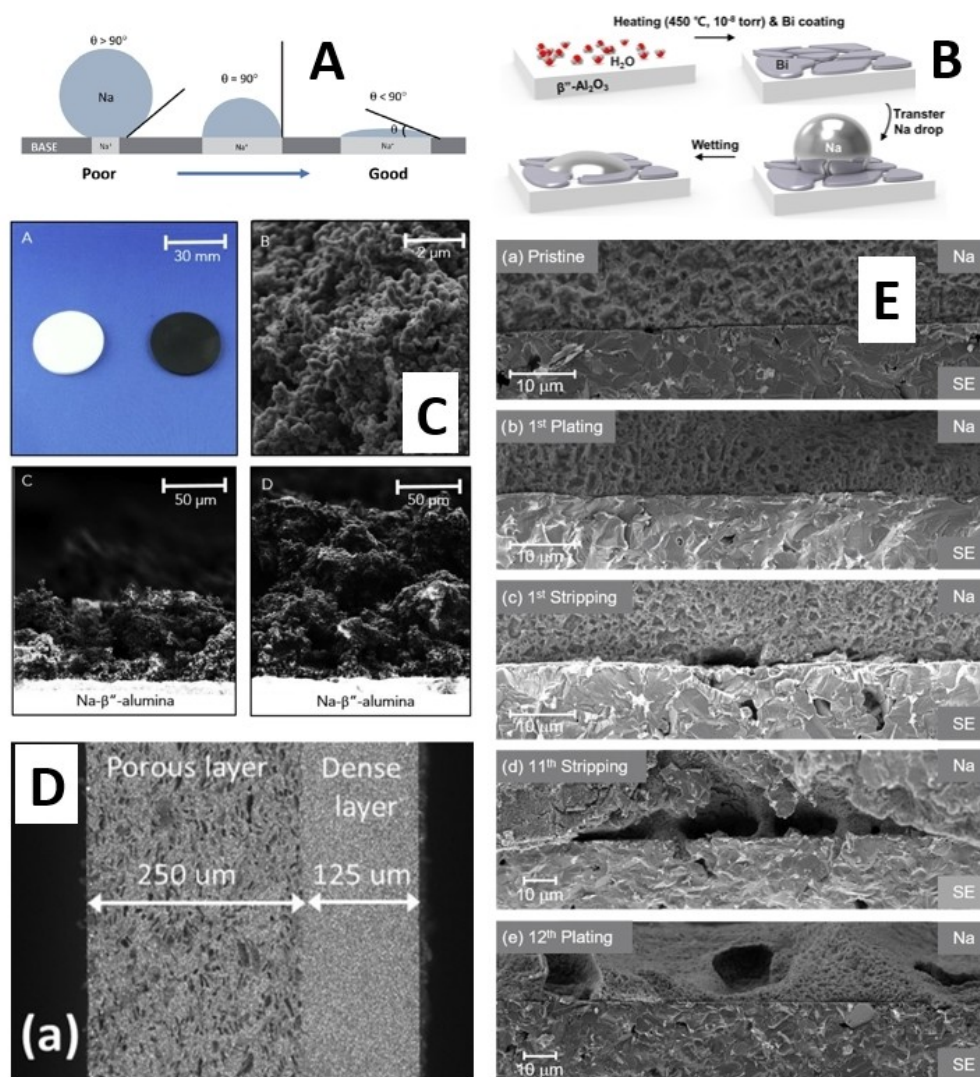
Figure 8. A) Schematic illustration of sodium drops on sodium-beta alumina with different wetting angles θ. Reproduced with permission from Ref. [116]. Copyright (2018) The Royal Society of Chemistry. B) Surface cleaning of sodium-beta alumina by heating with subsequent Bi thin film deposition by sputtering, followed by the liquid Na wetting test on the surface of sodium-beta alumina. Reproduced with permission from Ref. [117]. Copyright (2019) American Chemical Society. (C—A) Photograph of sintered sodium-beta alumina (left) and disk with sprayed carbon coating (right). (C—B) SEM image of the porous carbon coating (C—C and D) Cross-sectional images of the carbon coating with 50 μm and 200 μm thicknesses, respectively. Reproduced from Ref. [118]. CC BY 4.0, Copyright (2020) The Authors, published by Elsevier Ltd. (D) Back scattering SEM images of fracture surfaces of the bilayer sodium-beta alumina with a porous layer thickness of 250 μm and a dense layer thickness of 125 μm. Reproduced with permission from Ref. [119]. Copyright (2018) Elsevier B.V. (E) Cross-sectional SEM images of the sodium-beta alumina interface when (E-a) pristine and after (E-b) 1st plating, (E-c) 1st stripping, (E-d) 11th stripping, and (E-e) 12th plating after cycling at 1.5 mA cm^{-2} and under 4 MPa pressure. Reproduced with permission from Ref. [120]. Copyright (2020) American Chemical Society.

were cast into two type sheets, resulting in a bi-layer sodium-beta alumina with 125 μm dense and 250 μm porous layers after calcination and sintering steps at 1600 °C (see Figure 8D). The wettability improvement and bi-layer BASE accounted for the increased energy efficiency of the Na/NiCl$_2$ cell system.[119] Lai et al. also improved a Na/BASE/Na$_3$V$_2$(PO$_4$)$_3$ cell with a vertically porous-dense bilayer structure. Their improvement focused mainly on the side of the positive electrode (see Section 6).[125] Another bilayer electrolyte was prepared by integrating sodium-ions as well as poly(ethylene oxide) (PEO) into a sol-gel synthesis. The cross-section of the bilayer showed three different areas: a dense layer with a thickness of around 50 μm to 100 μm, porous bulk material, and in between a

sodium-enriched layer with a thickness of around 300 μm.[126] However, neither carbon coating nor bilayers may be needed for an improved ASR$_{cell}$. Simple heat treatment of polished sodium-beta alumina successfully reduced the ASR$_{NEI}$ due to the reduction of the number of hydroxyl groups at the interface. The ASR$_{NEI}$ decreased from 19,900 to just 8 Ω cm^2 in a Na/BASE/Na cell at room temperature (Figure 9A and B).[106]

Similar results were obtained with heat treatment from Bruce's group. Here, the resistance was lowered from roughly 15,000 Ω to 200 Ω for a Na/BASE/Na cell at 30 °C. It was ascribed to a reduction in surface hydroxides and carbonate species, as they occur on alkali-rich oxides.[120] With this simple measure, Bay et al. managed to increase the critical current
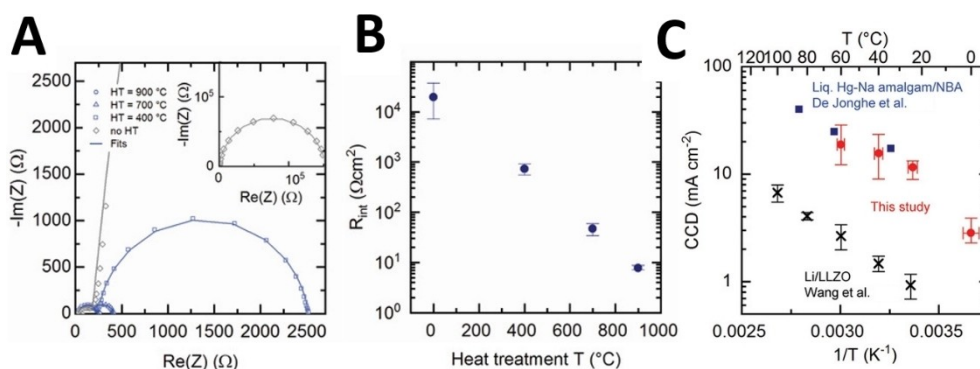
Batteries & Supercaps

Review
doi.org/10.1002/batt.202100131

Chemistry
Europe
European Chemical
Societies Publishing

Figure 9. A) Impact of heat treatment on interfacial resistance at room temperature. Representative Nyquist Plots, where the markers represent experimental data and lines represent fitted data. B) Interfacial resistance as a function of heat treatment temperature. C) CCD of the sample heat-treated at 900 °C in red in comparison with literature. For references, please check the original source. All figures reproduced from Ref. [106]. CC BY-NC-ND 4.0. Copyright (2019) The Authors, published by WILEY-VCH Verlag GmbH & Co. KgaA.

density (CCD), which is defined as the maximum available current density[127] of a solid-state battery. The CCD is related to a short-circuit due to dendrite growth and therefore, a crucial metric. An initial pressure of 3.4 MPa was applied for the assessment of the CCD. The CCD was increased from 0.3 mA cm^{-2} to 12 mA cm^{-2} for a charge density of 0.25 mAh cm^{-2} after heat treatment of the BASE and resistance reduction in the Na/BASE/Na cell at room temperature. This value is one of the highest reported CCD for a solid electrolyte.[106] For comparison, this value is ten times higher than the measured CCD of Li metal and $Li_7La_3Zr_2O_{12}$ (LLZO) at identical measurement conditions (1 mA cm^{-2}) and therefore, high enough for applications like electric vehicles (> 3 mA cm^{-2}) (Figure 9C).[128] The remarkable result highlights the potential of sodium solid-state batteries with modified sodium-beta alumina, which can be charged ten times faster than lithium solid-state batteries based on LLZO. It shows that the maximum current density is related to the interfacial resistance between the metal negative electrode and the SE. Those results demonstrate that an all-solid-state sodium battery based on sodium-beta alumina becomes a promising option when an appropriate positive electrode is available.[106]

In a three-electrode study, the processes of plating and stripping were separated in a Na/BASE/Na cell at room temperature, which undoubtedly deepens the understanding of the interface processes between a sodium metal electrode and sodium-beta alumina electrolyte. Na worked both as counter, reference, and the working electrode. Void formation in the Na metal at the interface occurred on stripping when the current density was too high. The voids grew over successive cycles (see Figure 8E). The growth was observed electrochemically as a voltage increase due to increasing polarization, as well as with cross-sectional SEM images and with operando tomography. The polarization on plating remained low and relatively constant, due to the uniform growth of sodium across the solid electrolyte, which partially occluded the voids which arose from previous stripping cycles. Hence, not all voids were filled in and the voids were pushed back away from the interface. This diminished the contact area of the sodium metal with the

electrolyte, which lead to high local plating currents and resulted in dendrite growth, and therefore, cell death. The tomography revealed that the total volume of voids grew with cycle number, which equals a decrease in the contact area between the sodium negative electrode and the solid electrolyte. Thus, the concept of a "critical current density of stripping" (CCS) was transferred from previous work on Li systems.[129] The CCS is defined as the current density, where sodium ion flux away from the interface exceeds the rate of replenishment of sodium to the interface due to diffusion and stress-driven deformation, i.e., creep. The latter is the dominant mechanism for sodium transport to the interface. Hence, void formation is driven by insufficient mass transfer towards the interface. Spencer Jolly et al. found that additional pressure successfully suppressed void formation. It was controlled throughout cycling. The pressure was applied on the aluminum spacers which were in contact with the sodium electrodes. Spring clamps and a piezoelectric load cell or a stage loading rig measured the pressure. The required pressure increased linearly with current density. However, this is not arbitrary gradable: If the current density exceeds the second critical current density (critical current density for plating, CCP), the formation of dendrites is inevitable, acting as "the ultimate power limit" of the cell system. The CCS is usually lower than CCP. The CCS was 1.5 mA cm^{-2} and 2.5 mA cm^{-2} for 4 MPa and 7 MPa in this system, respectively. However, those are not intrinsic values, due to differences in the purity of different surfaces of the SE, illustrating the importance of pre-treatment of the SE once more.[120] Hence, the values of 2.5 mA cm^{-2} and the previously mentioned 12 mA cm^{-2} do not contradict each other. The three-dimensional time-dependent model from Zhang et al.[130] showed excellent agreement with the experimental results from Spencer Jolly et al.[120] for an effective Na hardness of 15 MPa. According to Zhang et al., a higher stack pressure does not always improve the fractional creep rate. The higher pressure induces a more homogeneous contact stress, which reduces the creep rate. Nevertheless, the model confirms the necessity of stack pressure to suppress voids at high current densities. According to Zhang et al., contact elastoplasticity

Batteries & Supercaps

Review
doi.org/10.1002/batt.202100131

Chemistry Europe
European Chemical
Societies Publishing

dominates the pressure dependency of void suppression rather than creep.[130]

Rees et al. observed sodium electrodes before and after dendritic growth in sodium-beta alumina in a Na/BASE/Na cell for the first time with ^{23}Na magnetic resonance imaging (MRI) (Figure 10A). The dendrite growth followed a "spalling morphology".[131] Kazyak et al. observed the spalling morphology as one type out of four different dendrite morphologies besides straight, branching, and diffuse.[132] The spalling morphology forms when the dendritic crack spreads back to the surface. This forms a surface fracture, which is often followed by a short circuit. Despite the voltage drop to 0 V (*i.e.*, short circuit), no traversing dendrite was observed. This was probably due to Joule heating originating from the high current, which removes the thin parts of the dendrite, making the dendrite difficult to observe. The full spin-spin (T_2) relaxation mapping took roughly 11 hours, completed on commercially available equipment.[131]

Another study found a correlation between interface deformation between a sodium electrode and a 500 μm thick sodium-beta alumina, and the formation of dendrites. Mechanically induced stress must be avoided to prevent the formation of cracks, which open the pathway to agglomeration of sodium and dendrite growth. X-ray imaging was utilized to reveal the cracking of the sodium-beta alumina (Figure 10B).[133]

Those results indicate an influence of pressure on the performance of a cell system operating with sodium as the metal negative electrode. Surprisingly, no comprehensive data for elastic and plastic properties of sodium metal at room temperature was available, until recently. The data reveals that the elastic modulus (3.9 GPa using nanoindentation,[134] 4.6 GPa using acoustic techniques[135]), the shear modulus (1.7 GPa[135]) as well as the bulk modulus (8.5 GPa[135]) of sodium metal are smaller than the moduli of lithium metal, according to the lower melting point. The plastic properties with a yield strength between 0.19 MPa and 0.28 MPa at a strain rate of 10^{-3} s^{-1} may explain the rate capabilities of sodium as the negative electrode.[135] The yield strength is 0.41 MPa, when it is taken as one-third the hardness for ductile metals.[136] The soft nature of sodium assists in maintaining a uniform deposit morphology and interface contact. Sodium creeps at a faster rate than lithium, which results in a higher rate capability.[134] This is in line with findings from Park et al. They showed that pure alkali

metals have CCDs that scale inversely to their yield stress.[136] The stress exponent value of sodium suggests that the rate-controlling mechanism is dislocation climb, which was also proposed for lithium.[134] Wang et al. connect the electrochemical quantity of current density due to its impact on the height change of the sodium metal with the strain rate. With increasing strain rate (*i.e.*, with higher current density), the sodium metal, behaving like a non-Newtonian fluid, becomes more difficult to deform. For charging, additional pressure may be put on the electrolyte because the sodium flux away from the surface is impeded. On discharge, maintaining contact with the electrolyte is more difficult. When applying sodium metal on a clean sodium-beta alumina surface, not only frictional forces but also adhesive forces may impede the sliding of sodium metal. The flow stress increased up to 40% compared to the measurement on oil-lubricated stainless steel, with the aforementioned major implications to the charging procedure.[135] Liu et al. observed Na dendrite growth in real-time in an extensive ETEM–AFM (environmental transmission electron microscopy – atomic force microscopy) study. They were able to measure the elastic-plastic properties of individual dendrites with different shapes and diameters (Figure 11). Na dendrites reached tensile strengths up to 203 MPa, which is more than 300 times higher than that of bulk sodium. It underlines the findings of earlier works[137] that Na creep through defects can lead to the failure of solid-state sodium cells. Hence, Liu et al. suggest reducing the flaw size to mitigate sodium dendrite-induced failure in sodium-based batteries.[138] The relation between pressure, dendrites, and flaw size is the subject of current research. In a Li-ASSB, Li crept between the SE's grains under a stack pressure of 10 MPa, and therefore, plating occurred.[139] Again, this is no intrinsic value as the threshold correlates with flaws in the solid electrolyte.[136] Notably, a fabrication pressure of 25 MPa allowed proper wetting of the solid electrolyte with Li and reduced the cell resistance significantly, even as the pressure was later released to a lower value.[139] Sodium dendrite growth in defects may occur at lower pressures already due to Na's lower yield stress compared to Li. The findings suggest an optimal stack pressure: The pressure must be high enough to prevent void formation and guarantee good interfacial contact. On the other hand, to prevent creep of the alkali metal between the grains of the solid electrolyte and, of course, BASE fracture, an upper-
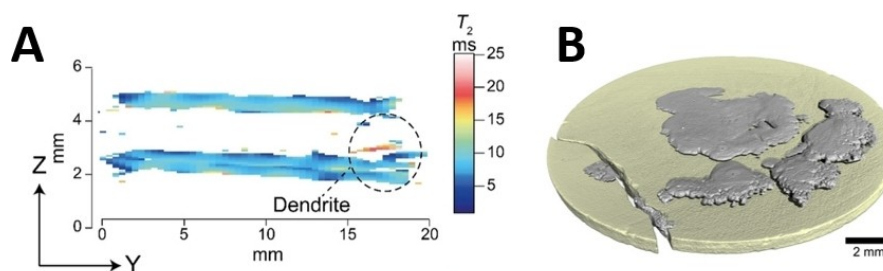

Figure 10. A) T_2 weighted contrast map of a Na/BASE/Na cell after short circuit due to a dendrite (highlighted). Reproduced from Ref. [131]. CC BY 4.0, Copyright (2020) The Authors, published by Wiley-VCH GmbH. B) 3D image obtained from ex situ X-ray microcomputed tomography of the solid electrolyte after short circuit of a Na/BASE/Na cell. Reproduced with permission from Ref. [133]. Copyright (2019) WILEY-VCH Verlag GmbH & Co. KGaA, Weinheim.
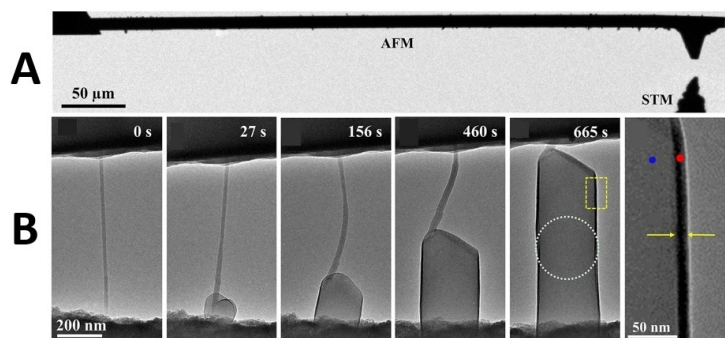
Batteries & Supercaps

Review
doi.org/10.1002/batt.202100131

**Chemistry
Europe**
European Chemical
Societies Publishing

Figure 11. A) TEM image of an AFM cantilever tip, which approaches the counter electrode of Na metal. The counter electrode is attached to a scanning tunneling microscopy (STM) probe. B) TEM images, which show the growth of a Na dendrite via electrochemical plating in timelapse. The yellow rectangle is magnified in the panel on the right. The yellow arrows indicate a 14 nm thick layer of Na_2CO_3, originating from the CO_2 atmosphere around the AFM tip, while the inner core is metallic sodium. Reproduced with permission from Ref. [138]. Copyright (2020) American Chemical Society.

pressure limit must not be exceeded. Those findings apply to temperatures below the melting point of sodium. However, for a high operating temperature of 250 °C, no dendrite formation was observed in a Na/BASE/Na cell, whose SE was carbon-coated, even at current densities as high as 2600 mA cm^{-2} and 10 Ah cm^{-2} cumulative plated capacity. The high temperature eliminated the creep-related mass transport limitations mentioned in the sections above. The temperature above the melting point of sodium provides a practical solution for the integration of sodium metal negative electrodes in Na/BASE cell systems.[118]

Summarized, utilization of sodium-beta alumina doesn't inevitably prevent dendrite growth in electrochemical cells, operated at room temperature, because the formation of dendrites is not only related to the sodium-beta alumina itself. The properties of the sodium metal negative electrode play a crucial role, too. To grasp the processes at the Na/BASE interface, it is important to understand the mechanical properties of both compartments. Moreover, sodium creep to the interface can be increased by applying pressure. Therefore, high fracture strengths of sodium-beta alumina are necessary, which shows the importance of mechanical stability. Dendrite growth in cell systems utilizing sodium as the negative electrode and sodium-beta alumina can be prevented when the CCS is not exceeded. Another possibility is an increase in temperature for cell operation, where the temperature exceeds the melting point of sodium.

6. Performance of Sodium-Based Cell Systems Utilizing Sodium-Beta Alumina and Modified Interfaces

Multiple groups recognized the potential of sodium-beta alumina in novel cell systems. The physical and (electro) chemical properties of sodium-beta alumina (BASE), *e.g.*, high ionic and low electronic conductivity, high mechanical strength, large electrochemical stability window, and stability against sodium, are capable of competing or even outperform-

ing those of the other solid electrolytes. Other electrolytes include NaSICON, chalcogenides, and complex hydrides, for example (compare Figure 12). However, high mechanical strength makes the assembly of a cell more difficult. These novels, medium- to low-temperature sodium-based cell systems most often utilize sodium as the negative electrode and sodium-beta alumina as a solid electrolyte. The sodium negative electrode is paired with a Na-ion type positive electrode. As this section will demonstrate, Na-ion type positive electrodes can be deployed successfully in medium- to low-temperature sodium-based cell systems, utilizing sodium-beta alumina as a solid electrolyte. The cell systems are presented in the next sections. They retrace the chronological order of these cell systems. From the presented literature, necessary parameters are shown in Table 3 to make the comparison of different cells easier,[140] providing a useful outline for the progress of those cell systems.

The importance of temperature regarding cell performance was demonstrated in early work on all-ceramic solid-state sodium full cell. Thin electrodes of P_2-$Na_{2/3}[Fe_{1/2}Mn_{1/2}]O_2$ and $Na_2Ti_3O_7$-$La_{0.8}Sr_{0.2}MnO_3$ with a thickness of only 22 μm and 52 μm were air sprayed on a 154 μm thin sodium-beta alumina. To enhance electronic conductivity in the negative electrode, $Na_2Ti_3O_7$ was blended with $La_{0.8}Sr_{0.2}MnO_3$. In this type of full cell setup (without sodium acting as sodium reservoir), Coulomb efficiency is even more important because sodium is not available in surplus. The elevated operating temperature of 350 °C helped to increase the ionic conductivity in the sodium-beta alumina and enhanced activity in the electrodes. Both decreasing the operating temperature to 250 °C as well as increasing the discharge current to a "C-Rate" of 2 h^{-1} diminished the specific discharge capacity from 152 mAh g^{-1} (0.05 h^{-1}, 350 °C) to 60 mAh g^{-1} due to increased polarization losses, which were already observable in the voltage profile. Another all-ceramic solid-state full cell with an electrolyte thickness of 195 μm in a voltage window from 1.0 V to 4.0 V showed good capacity retention over 100 cycles (Figure 13A).[141] This result of the early work indicates the difficulty of lowering the operating temperature of cell systems in an all-
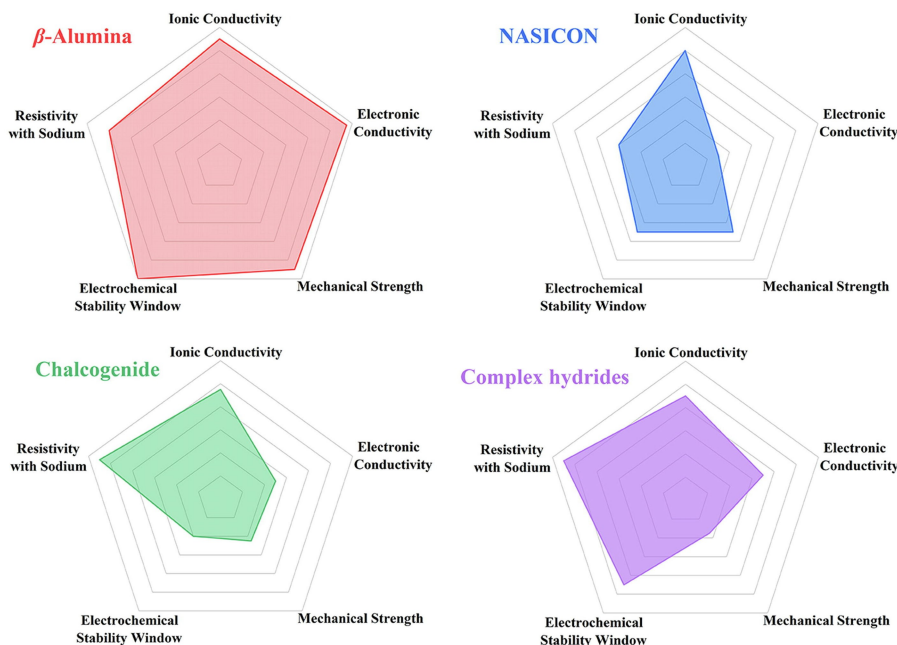
Batteries & Supercaps

Review
doi.org/10.1002/batt.202100131

Chemistry
Europe
European Chemical
Societies Publishing

Figure 12. Radar plots of four different solid electrolytes and their various physical and chemical properties. Reproduced with permission from Ref. [18]. Copyright (2020) Elsevier Ltd.

Table 3. Characteristic cell values of the novel, medium- to low-temperature cell systems based on sodium-beta alumina and Na-ion type positive electrodes*.

Cell components NE/Electrolyte/PE	U [V]	I_{spec} [mA g^{-1}]	$q_{dis, end}$ [mAh g^{-1}]	Cycles	q_{ret} [%]	T [°C]	A [cm^2]	m_{active} [mg cm^{-2}]	$m_{active}/m_{positive}$ [wt%]	U_{avg} [V]	E_{active} [Wh kg^{-1}]	$E_{positive}$ [Wh kg^{-1}]	ASR_{cell} [Ω cm^2]	Rate test [mAh g^{-1} @ h^{-1}]
Na/BASE/Na$_3$V$_2$(PO$_4$)$_3$ [124]	2.5–3.7	23	**100**	100	100	58	1.1	3.00	60	n.a.	n.a.	n.a.	821	**100 @ 0.1** 80 @ 0.5
Na−Sn/BASE/PTO-PEO [149]	**1.3–3.0**	41	290	50	80	60	1.3	1.20	30	2.15	623	187	693	**360 @ 0.1** 180 @ 0.5
Mg/BASE/Na$_{1.5}$VPO$_{4.8}$F$_{0.7}$ [148]	2.4–3.8 (vs. Mg)	130	98	20	85	25	30.7	n.a.	72	3.06	300	216	n.a.	110 @ 0.2 80 @ 2
Na/BASE/NaTi$_2$(PO$_4$)$_3$ [142]	1.5–2.5	13	100	50	75	25	2.5	0.40	70	1.98	198	138	9,398	130 @ 0.1 60 @ 0.5
Na$_2$Ti$_3$O$_7$-La$_{0.8}$Sr$_{0.2}$MnO$_3$/BASE/NaFMO [141]	1.0–4.0	13	**140**	10	92	350	2.5	n.a.	100	2.27	318	318	n.a.	**140 @ 0.1** 67 @ 2
Na/ANs-GPE/Na$_3$V$_2$(PO$_4$)$_3$ [150]	2.5–3.8	171	86	500	95	25	2.5	2.8	70	n.a.	n.a.	n.a.	375 (60 °C)	**90 @ 0.1** 65 @ 2
Na/NP-GPE/Na$_3$V$_2$(PO$_4$)$_3$ [151]	2.5–4.0	59	80	300	85	25	1.1	1.28	80	3.19	255	204	456	97 @ 0.2 68 @ 2
Na/BASE/Na$_2$FeP$_2$O$_7$ [152]	2.0–4.3	8	70	623	87	30	1.0	0.60	72	2.77	193	139	n.a.	70 @ 0.01 24 @ 0.1 (m_{active} = 4 mg cm^{-2})
Na/BASE/Na$_2$FeP$_2$O$_7$ [153]	2.0–4.5	10	80	1	100	30	1.0	3.68	83	n.a.	n.a.	n.a.	120	80 @ 0.1 47 @ 2
Na/BASE/Na$_3$V$_2$(PO$_4$)$_3$ [73]	2.5–4.0	59	64	100	79	60	2.0	n.a.	80	3.00	191	153	n.a.	**92 @ 0.2** 65 @ 2
Na/BASE/Na$_{0.66}$NMO + IL [143]	2.5–3.8	528	52	10,000	90	70	n.a.	2.0	40	3.30	172	69	80 Ohm	80 @0.1 73 @ 2
Na/BASE/Na$_3$V$_2$(PO$_4$)$_3$ [125]	2.8–4.0	11.7	83	100	96	60	n.a.	8.0	100	3.25	270	270	115 Ω	87 @ 0.1

*Italic values are calculated from data given in the publication but are not explicitly mentioned. Bold values are estimated from graphs or figures. U: voltage window, I_{spec}: specific current, $q_{dis, end}$: specific discharge capacity at the end of cycling, Cycles: number of cycles, q_{ret}: capacity retention, T: temperature of cell operation, A: surface area, m_{active}: loading of the active material in the positive electrode, $m_{active}/m_{positive}$: Mass fraction of active material in the positive electrode, U_{avg}: Average voltage in the last discharge after the number of cycles "Cycles", E_{active}: Specific energy in regard to the mass of the active material in the positive electrode, $E_{positive}$: Specific energy in regard to the mass of the positive electrode, ASR_{cell}: area-specific resistance of the cell, Rate test: Rate performance of the cell system, given in specific discharge capacity at two different rates.

ceramic solid-state cell while maintaining electrochemical performance.

Lowering the operating temperature is easier, when auxiliary materials are used, as it was in a Na/BASE/NaTi$_2$(PO$_4$)$_3$ cell, where the temperature of cell operation was lowered to

just 25 °C. In this work, the positive gel-type electrode (NaPF$_6$ in EC/DMC and PVDF-HFP) was screen-printed with an approximate thickness of 60 μm on the ceramic electrolyte. Sodium-beta alumina with a thickness of 100 μm was applied via tape-casting and subsequent sintering process. A tight attachment
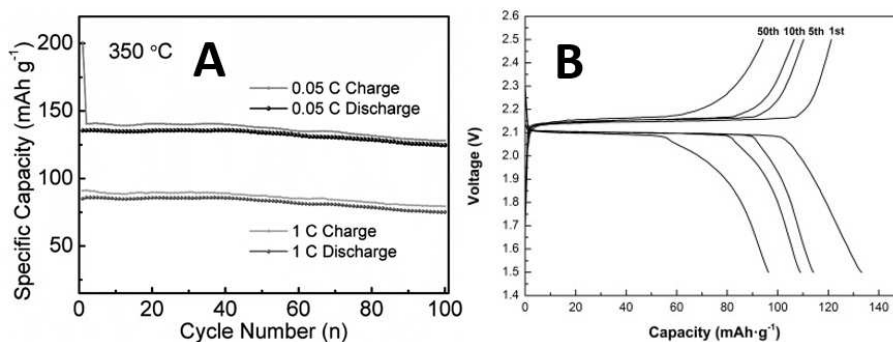
Batteries & Supercaps

Review
doi.org/10.1002/batt.202100131

Chemistry Europe
European Chemical
Societies Publishing

Figure 13. A) Cycling performance of the all-ceramic $Na_2Ti_3O_7$-$La_{0.8}Sr_{0.2}MnO_3$/BASE/P_2-$Na_{2/3}[Fe_{1/2}Mn_{1/2}]O_2$ cell. Reproduced with permission from Ref. [141]. Copyright (2014) WILEY-VCH Verlag GmbH & Co. KgaA. B) Charge and discharge curves of the Na/BASE/$NaTi_2(PO_4)_3$ cell system with a voltage plateau at around 2.15 V (Reproduced with permission from Ref. [142]. Copyright (2016) Elsevier B.V.

of the positive electrode to the sodium-beta alumina was observed from SEM imaging. It was assumed that the gel-type electrode helped to obtain a low interfacial polarization. No impedance spectra were recorded to prove this claim. However, the charge/discharge profiles showed a broad, flat, and stable voltage plateau at 2.15 and 2.10 V, respectively, at $0.1\,h^{-1}$ (Figure 13B). However, the internal cell resistance was still extensive, as it was calculated via Ohms law from the over-voltage given in the voltage profile (see Table 3). The intrinsic polarization from the negative electrode may be significant, especially since the interface on the side of the negative electrode was not modified.[142] The work shows that an operation at room temperature is possible. However, a thin electrolyte in cell systems based on sodium-beta alumina is not sufficient to provide low resistance at room temperature, and thus, good rate performance. Interface modifications on both sides of sodium-beta alumina are necessary.

A strategy to tackle interface issues was the wetting of the electrolyte/electrode interface with an ionic liquid (IL). Apparently, the IL enables are more facile charge transport in comparison to the gel-type approach due to even better interfacial contact with BASE. It is likely that the polymer of the gel-type electrode induced additional resistance (compare Table 3), especially at the operation temperature of 25 °C. The IL, PY14FSI, enlarged the contact area between the transition

metal positive electrode made from the active material $Na_{0.66}Ni_{0.33}Mn_{0.67}O_2$ (NaNMO) and sodium-beta alumina. It lowered the interface impedance by enhancing the contact area between electrode and electrolyte. The resulting soft positive electrode adhered directly onto the sodium-beta alumina pellet (Figure 14A). It was assumed that the adhesion promoted the ionic transport, leading to outstanding cycling stability of the new type of solid-state cell of more than 10,000 cycles at $6\,h^{-1}$ and a final specific discharge capacity of $52\,mAh\,g^{-1}$ at 70 °C (Figure 14B). The addition of the IL significantly reduced the resistance in impedance measurements, which shows the importance.[143] A similar method was already successfully employed in a Na/NASICON/$Na_3V_2(PO_4)_3$ cell with PP13FSI.[144] The remarkable results suggest further research on the combination of sodium-beta alumina, ionic liquids, and transition metal oxide positive electrodes. For cell systems utilizing transition metal oxides in the positive electrode, calcium impurities may be detrimental to the performance of the cell system. The harmful effect of calcium on sodium-beta alumina was reported already by several researchers.[145] As it was shown for $NaCoO_2$ thin-film electrodes recently, calcium impurities migrate from the sodium-beta alumina bulk to the thin film. For layers thinner than 9.0 nm, spectroscopic XPS data indicates a mixed oxide formation (CaO-Al_2O_3) in the interface region, presumably $CaAl_2O_4$. Thus,
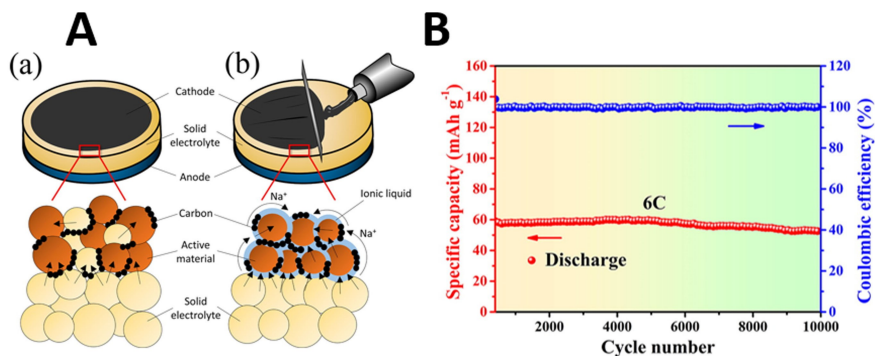

Figure 14. A) Schematic diagram of A-a) a conventional sintering type, and A-b) the novel cell system with the ionic liquid and sodium-beta alumina. Reproduced with permission from Ref. [143]. Copyright (2016) American Chemical Society. B) Cycling performance of the cell system with over 10,000 cycles at $6\,h^{-1}$. Reproduced with permission from Ref. [143]. Copyright (2016) American Chemical Society.

Batteries & Supercaps

Review
doi.org/10.1002/batt.202100131

Chemistry Europe
European Chemical
Societies Publishing

the ionic conductivity decreases at the interface. For thicker electrodes, an ion-exchange mechanism takes place, i.e., calcium replaces sodium in the layered transition metal oxide. Both processes are detrimental to interface kinetics and may hinder the electrochemical performance of the cell system.[146] A Na/BASE/Na_xCoO_2 cell was further investigated with XPS and XRD. Again, a $CaAl_2O_4$ phase was observed at the BASE/positive electrode interface. A $Ca_3Co_4O_9$ phase was formed by the transfer of Ca^{2+} via the intermediate $Na_xCa_yCoO_2$ phase, which can result in full conversion of the positive electrode into $Ca_3Co_4O_9$. Impedance measurements, as well as electrochemical cycling showed that these interphases result in high over-voltages and small discharge capacities. However, due to the thin-film positive electrode, sodium-beta alumina acted as an unlimited calcium reservoir. Hence, the results may not be transferable to typical bulk batteries.[147]

Different methods for negative electrode interface modification were already presented in section 5. The positive impact of this modification on cell performance was demonstrated with a thin film composed of cotton-cloth-derived disordered carbon tubes (DCTs) on the sodium-beta alumina surface, which reduced the interfacial resistance in a Na/Na-cell. Furthermore, the advantage of the modified interface was demonstrated in a Na/DCT-BASE/$Na_3V_2(PO_4)_3$ cell. The operating temperature of 58 °C was far below the sodium melting point (98 °C). The interfacial contact of Na/DCT-BASE remained quite stable even after 100 cycles. Due to the modification, the ASR_{NEI}, which was ascribed to the negative electrode side, increased by only 51 to 228 $\Omega\,cm^2$ after 100 cycles, while the

ASR_{PEI} ascribed to the side of the positive electrode more than doubled to 577 $\Omega\,cm^2$ (Figure 15A). A final specific discharge capacity of 100 $mAh\,g^{-1}$ was reached, without evident loss of specific capacity over cycling. However, the cell showed a poor rate performance, which may be related to the increased intrinsic polarization, mainly induced by the positive electrode interface, which was not modified.[124]

Both the negative and the positive sides of the sodium-beta alumina were modified for a reduced interfacial resistance in a proof-of-concept study. It demonstrated the combination of an organic quinone-based positive electrode (pyrene-4,5,9,10-tetraone, PTO) with sodium-beta alumina and sodium as the negative electrode at 60 °C. Between the sodium negative electrode and sodium-beta alumina, a 20-nm-thick Sn thin interlayer was deposited in a thermal evaporator, while a PEO-PTO composite positive electrode was utilized that formed both ionic and electronic pathways (Figure 15C). Both modifications drastically reduced the interfacial resistance, showing that interface modifications are important for cell systems at the side of the positive electrode, too. These modifications successfully ameliorated the interface challenges and enhanced cycling stability. Due to the quinone-based positive electrode and its corresponding cell reaction, a high initial discharge specific capacity of 362 $mAh\,g^{-1}$ was achieved, which results in an initial specific energy of around 900 $Wh\,kg^{-1}$ (considering only active material mass) due to the average voltage of 2.46 V vs. Na/Na^+ during discharge at 60 °C.[149]

An even higher average discharge voltage was obtained by another proof-of-concept cell system, which was an Mg/Na
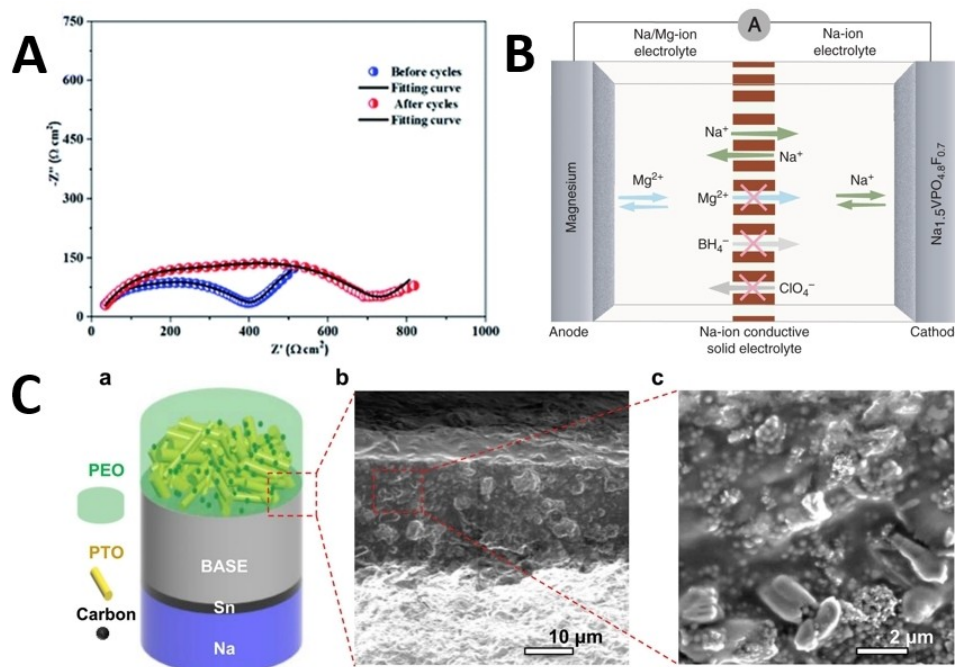

Figure 15. A) Nyquist plot of the Na/DCT-BASE composite and the Na/BASE cell before (straight line) and after (dotted line) 100 cycles. Reproduced with permission from Ref. [124]. Copyright (2018) The Royal Society of Chemistry. B) Working principle of the high-voltage Mg/Na dual ion battery. Reproduced from Ref. [148]. CC BY, Copyright (2019) The Authors, published by Springer Nature. (C-a) Schematic illustration of the Na–Sn/BASE/PTO-PEO cell, and (C-b and c) highlight the intimate contact between the positive electrode and sodium-beta alumina as well as the network between PTO-PEO in the composite electrode. Reproduced with permission from Ref. [149]. Copyright (2019) Elsevier Ltd.

Batteries & Supercaps

Review
doi.org/10.1002/batt.202100131

**Chemistry
Europe**

European Chemical
Societies Publishing

dual-ion cell. These cells generally consist of an Mg metal negative electrode, a Na-ion positive electrode, and a liquid Mg/Na dual-ion electrolyte. Hence, the electrolyte must support reversible plating of Mg on the negative electrode as well as insertion/removal of Na^+ at the positive electrode, which often limits the voltage range. Kravchyk et al. proved in a modified Mg/Na dual-ion cell (Mg/dual-ion electrolyte/BASE/sodium-ion electrolyte/$Na_{1.5}VPO_{4.8}F_{0.7}$) that a high voltage is achievable due to utilization of oxidatively stable, liquid Na-ion electrolyte in the vicinity of the positive electrode separated from the Na/Mg-ion electrolyte in the vicinity of the negative electrode by sodium-beta alumina (Figure 15B). The concept resulted in a cell with a high average discharge voltage of 3.0 V vs. Mg/Mg^{2+} at a rate of 1 h^{-1}. The specific capacity was 98 mAh g^{-1} after 20 cycles. A limiting factor in this cell concept was the solubility of the Mg-salt magnesium borohydride in tetraglyme in the Mg/Na dual-ion electrolyte, as it limits the negative electrode capacity associated with reversible magnesium stripping/deposition. For improved performance, Mg/Na dual-ion electrolytes with higher Mg^{2+} molarity are needed.[148]

Instead of making the electrodes more viable to fit the rigid electrolyte, the advantages of sodium-beta alumina were employed while making the electrolyte itself smoother. An inorganic ionic conductor/compact gel polymer electrolyte (GPE) composite with cross-linked sodium-beta alumina nanowires (ANs) was fabricated.[150] The ANs were compactly coated with a polymeric poly(vinylidene fluoride-co-hexafluoropropylene) (PVDF-HFP) layer. This resulted in a dense, but flexible membrane structure with a thickness of 80 μm, which showed high electrochemical stability up to 4.8 V vs. Na/Na^+. The composite electrolyte exhibited solid-liquid hybrid Na^+ transportation channels due to the cross-linking of ANs inside the membrane, as it was observed via SEM imaging. It enhanced not only the transportation of Na^+ but also the mechanical strength of the composite electrolyte (Figure 16A). Consequently, the ANs induced a uniform deposition of Na metal, leading to a long-term cycling performance over 1000 cycles at 1 h^{-1} at room temperature in a Na/ANs-GPE/$Na_3V_2(PO_4)_3$ cell system without any side reactions or dendrite growth. The cell with an NVP mass loading of 2.8 mg cm^{-2} still showed 86 mAh g^{-1} after 500 cycles (Figure 16B). However, the membranes were soaked in a liquid electrolyte, and a thin but stable SEI layer was formed on the positive electrode. Additionally,

the overvoltage was only 0.18 V despite the ionic conductivity of the composite electrolyte of only 7.9×10^{-4} S cm^{-1} at room temperature. The overvoltage is significantly lower than other room temperature overvoltages due to sufficient contact and affinity with both the positive as well as the negative electrode (compare Table 3). The transport number of sodium ions t_{Na}^+ was determined as 0.37. ^7Li and ^{23}Na NMR spectra as well as XRD data indicated the strong participation of ANs at the ionic transport. The ANs formed transportation channels through as well as along the ANs in the composite electrolyte.[150] Liu et al. obtained a similar Na/NP-GPE/$Na_3V_2(PO_4)_3$ cell performance with a PVDF-HFP/poly(methylmethacrylate)-based GPE containing 4 wt% sodium-beta alumina nanopowder (NP).[151]

Yamauchi et al. established a strong junction at the positive electrode and electrolyte interface by cofiring $Na_2FeP_2O_7$ (NFP) crystallized glass and beta alumina solid solution at 550 °C. To obtain the crystalline phase of NFP, heat treatment in reducing H_2/N_2 atmosphere was necessary. The glass-ceramic positive electrode, which was also highly resistant to overcharging, showed stable cycling performance with a high capacity retention of 87% over more than 600 cycles (Figure 17A). However, the voltage profile leads to the assumption of high internal resistance, which may be the reason the Na/BASE/NFP all-solid-state cell was evaluated only at 0.1 h^{-1}.[152] Even though no resistances were given, Yamauchi et al. repeated the cell preparation with a mass loading of 3.9 mg NFP and reported an internal resistance of 3929 Ω at a depth-of-discharge (DOD) of 45%, measured during charge/discharge reaction via operando impedance spectroscopy. This was the minimum value for this cell since the resistivity components varied significantly during cycling, especially the charge transfer resistivity attributed to the positive electrode. The dependency on the charge depth was explained as followed: During charging, Na-ions are depleted in the NFP and released from the interior of the active material particles. During discharging, the NFP is saturated with Na-ions, which occupy the free space where Na-ions are able to move. In four follow-up experiments, the Na/BASE/NFP cell was continuously improved by lowering the crystallization temperature and either adjusting the conductive additive content, roughening the sodium-beta alumina surface, or decreasing the particle size. A decrease in crystallization temperature supported the formation of conduction paths, hence increasing the ionic conduction at the active
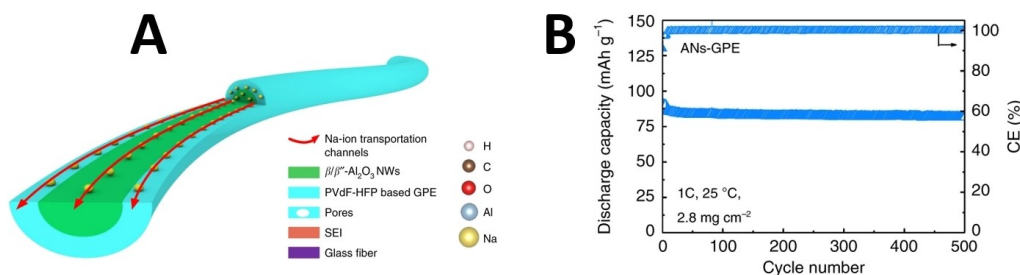

Figure 16. A) Scheme of the ion transport through and along the ANs. Reproduced from Ref. [150]. CC BY 4.0, Copyright (2019) The Authors, published by Springer Nature. B) Cycling performance of Na/ANs-GPE/NVP cell with NVP loading of 2.8 mg cm^{-2} at 25 °C. Reproduced from Ref. [150]. CC BY 4.0, Copyright (2019) The Authors, published by Springer Nature.

Batteries & Supercaps

Review
doi.org/10.1002/batt.202100131

Chemistry
Europe
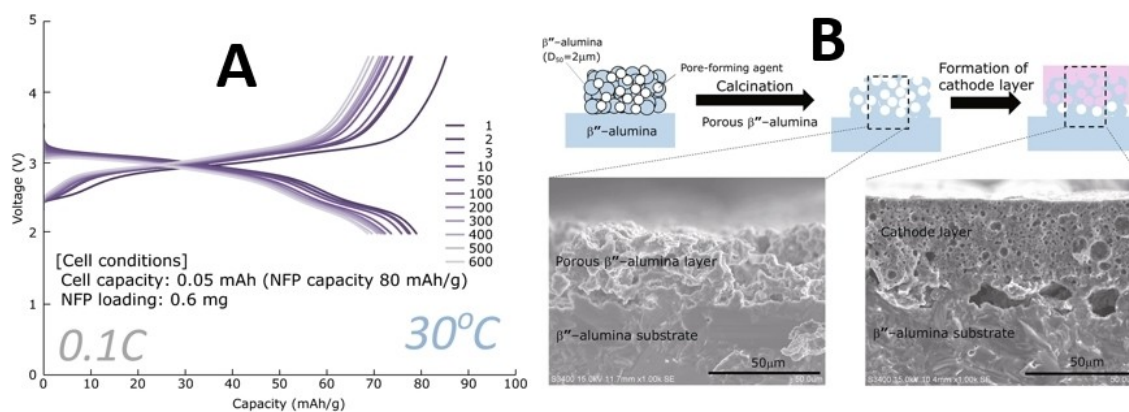European Chemical
Societies Publishing

Figure 17. A) Charge and discharge curves of the pressureless Na/BASE/NFP all-solid-state cell. Reproduced with permission from Ref. [152]. Copyright (2019) The American Ceramic Society. B) Illustration of the preparation of the roughened sodium-beta alumina surface and SEM images of the BASE/positive electrode interface. Reproduced from Ref. [153]. CC BY 4.0, Copyright (2020) The Authors, published by Springer Nature.

material/BASE interface. An increase in the contact area of the interface between NFP and sodium-beta alumina or conductive additive assisted the diffusion for Na-ions and electrons in the NFP. Roughening both sides of the sodium-beta alumina surface also increased the solid electrolyte-electrode layer interface and lowered the internal resistance subsequently to only 120 Ω at a DOD of 29% (Figure 17B). The interface characteristics are comparable to those of a liquid electrolyte-based Li-ion and sulfide-based all-solid-state battery. The cells were tested especially regarding their rate characteristics. It was proven that the rate characteristics improved with decreasing internal resistance. The Na/BASE/NFP cell, in which both surfaces were roughened, showed a superior rate performance in comparison to the original cell system and was discharged at a rate of 10 h^{-1}. A pouch cell with an adjusted amount of conductive additive operated at 0 °C and even −20 °C, which is a significant result when considering the low ionic conductivity of sodium-beta alumina at this temperature.[153] This result should ultimately exile the misconception that cells utilizing sodium-beta alumina work only at elevated temperatures. The comparison of the two cells with the NFP positive electrodes in Table 3 shows that the roughening of the sodium-beta alumina enabled a six times higher loading of NFP active material, without decreasing the specific capacity. Hence, higher energy densities are possible with this measure.

Yamauchi et al. roughened the surface of sodium-beta alumina to increase the BASE/electrode interface. Lai et al. increased the BASE/positive electrode interfacial contact by preparing a 1050 μm thick BASE with a porous-dense bi-layer structure by the ice-templet method. The vertically porous layer was 960 μm thick and exhibited pore diameters in the range of 10–20 μm. The porous layer with a porosity of 46% was carbon-coated and infiltrated with a mass-loading of 8 mg cm^{-2} Na$_3$V$_2$(PO$_4$)$_3$ (NVP). 8 mg cm^{-2} is the highest mass loading of all presented cell systems in Table 3. Hence, the specific energy in regard to the mass of the positive electrode is one of the highest values (270 W kg^{-1}). Liquid electrolyte was added to wet the interface. The resulting Na/BASE/NVP cell showed a

specific discharge capacity of 83.1 mAh g^{-1} after 100 cycles with a retention of 96% at 60 °C. The resistance was about 115 Ω, which is 1/20 of the resistance of the reference cell.[125] Unfortunately, Lai et al. performed no rate test and gave no cell area. The claim that the dense layer might prevent dendrites is doubtable, considering the findings in Section 5. However, Lai et al. confirmed with the bi-layer approach the findings from Yamauchi et al.: Increasing the interface contact area provides enhanced electronically and ionically conductive pathways, although two different positive electrode materials were utilized.

7. Summary and Outlook

This review provided an overview of the development of the ceramic sodium-beta alumina solid electrolyte and its application in novel, medium- to room-temperature sodium-based batteries with Na-ion type positive electrodes. While sodium-beta alumina is already successfully used in high-temperature batteries, recent research shows that it can be a promising material for solid-state batteries (SSBs), too. Sodium-beta alumina meets important requirements for SSBs such as high ionic conductivity, negligible electronic conductivity, chemical, thermal, and mechanical stability, environmental friendliness as well as non-toxicity. Room temperature ionic conductivity is no limiting factor anymore, as it reaches values of around 5 mS cm^{-1} nowadays. For fabrication, methods with low sintering temperature besides conventional solid-state synthesis are of interest to produce thin but mechanically stable ceramics with high grain conductivity and low grain boundary resistance. BASE's thickness in most cell concepts is around 0.5–1 mm. A thin electrolyte is essential for a low area-specific resistance of the electrolyte (ASR$_{electrolyte}$) and thus of the cell (ASR$_{cell}$). However, a low ASR$_{electrolyte}$ was not a decisive factor in the presented cell systems. The reason is that ASR$_{electrolyte}$ is negligible, with decent ionic conductivities already. Hence, cells with a thin electrolyte did not automatically show a better electrochemical performance than cells with thicker electro-

Batteries & Supercaps

Review
doi.org/10.1002/batt.202100131

Chemistry Europe
European Chemical
Societies Publishing

lytes. Nonetheless, the BASE should be as thin as possible to maximize energy efficiency. However, the thickness reduction might be limited by mechanical stability. Adequate dopants should be considered to enhance not only the ionic conductivity but also reduce sintering temperatures.

For batteries using sodium as the negative electrode, sodium-beta alumina as solid electrolyte, and Na-ion type positive electrodes, attention must be paid to the area-specific resistance (ASR_{cell}), which is a critical performance parameter, affecting the overall cell performance. The $ASR_{electrolyte}$ can be lowered by dopants and by the fabrication method. For sodium-beta alumina, $ASRs_{electrolyte}$ around $1\,\Omega\,cm^2$ were reached already. Sodium-beta alumina's rigid interfaces can lead to high resistance. This applies to the positive as well as negative electrode/electrolyte interface. Intimate contact of the positive Na-ion type electrode with BASE must be established to minimize the area-specific resistance related to the interface of the positive electrode (ASR_{PEI}). Here, ionic liquids (IL) and gel polymer composites offer huge potential for modification of the interface, as the number of available materials is vast and their properties as well as results of former experiments, which utilized these additives, are promising. Although the use of ILs and gels is a step back from true "solid-state" batteries, they might lead to significant improvement in electrode performance. For the BASE/negative electrode interface, low-cost approaches to mitigate poor wetting are needed, such as carbon coating or simple heat treatment. These measures lower the area-specific resistance related to the interface of the negative electrode (ASR_{NEI}). Suitable interface engineering shifts the critical current density (CCD), which is another crucial parameter for medium- to low-temperature sodium-based cell systems, to higher values. This allows faster charge- and discharge, *i.e.*, higher power densities. In fact, the CCD of cells utilizing sodium metal and sodium-beta alumina at room temperature is one magnitude higher ($12\,mA\,cm^{-2}$) than the measured CCD of lithium metal and $Li_7La_3Zr_2O_{12}$ (LLZO) at identical measurement conditions. To avoid cell death, literature underlines the importance of strict pressure management for room temperature operations. Research papers should include information on whether the pressure is applied during fabrication (fabrication pressure) or cycling of the cell system (stack pressure). External pressure shifts the CCD to higher values. For sodium-based batteries, an optimal stack pressure might exist. The external pressure, as well as the pressure due to volume changes of the electrodes, must be taken into account when considering the thickness of the electrolyte. However, no cell failure was reported due to volume changes of the electrodes yet. Generally, important variables and a set of necessary parameters must be controlled and reported more precisely, *e.g.*, pressure in the cell system, cell area, and average voltage. These parameters are required to benchmark and compare the cell performance.[140]

Elevated temperatures increase BASE's ionic conductivity and thus overall cell efficiency due to lower ASR_{cell}. Concerning interface kinetics and to bypass current limitations and dendrite growth, elevating the temperature above the melting point of sodium may be advantageous. While this might be a strategy for realizing stationary batteries, an operating temperature window from about $-20\,°C$ to $50\,°C$ is required for mobile applications. None of the studies published so far satisfy this requirement, and most measurements are conducted at elevated temperatures (typically $25\,°C$ to $70\,°C$). Improvements towards lower temperatures are therefore needed. Next-generation all-solid-state cells based on BASE must utilize an electrolyte thick enough to withstand external pressure for a high CCD while exhibiting low $ASR_{electrolyte}$ due to high ionic conductivity. Cost-efficient interface modifications are required for the BASE/positive electrode as well as the BASE/negative electrode interface to lower the values for ASR_{PEI} and ASR_{NEI}. These measures result in a low ASR_{cell} and therefore ensure cell performance with high efficiencies. Sodium batteries with Na-ion type positive electrodes and sodium-beta alumina as electrolytes showed already 10,000 cycles at high specific currents. They were able to operate from 1.0 V as lower cut-off voltage up to 4.5 V vs. Na/Na$^+$. The operating temperatures ranged from ambient temperature up to $350\,°C$, but they even operated at temperatures as low as $-20\,°C$.

Overall, sodium-beta alumina as a solid electrolyte is regaining prominent interest thanks to the development of solid-state batteries. As the most important advantage, sodium-beta alumina is environmentally friendly, based on abundant elements, and shows excellent mechanical properties. Combined with the latest progress in materials and interface design, the use of this ceramic for solid-state batteries in mid- to low-temperature applications may become a very attractive option for the future.

Acknowledgements

Conflict of Interest

The authors declare no conflict of interest.

[1] S. Chu, A. Majumdar, *Nature* **2012**, *488*, 294.
[2] a) M. H. Mostafa, S. H. Abdel Aleem, S. G. Ali, Z. M. Ali, A. Y. Abdelaziz, *J. Energy Storage* **2020**, *29*, 101345; b) O. Schmidt, S. Melchior, A. Hawkes, I. Staffell, *Joule* **2019**, *3*, 81.
[3] A. R. Dehghani-Sanij, E. Tharumalingam, M. B. Dusseault, R. Fraser, *Renewable Sustainable Energy Rev.* **2019**, *104*, 192.

[4] J. Janek, P. Adelhelm in *Handbuch Lithium-Ionen-Batterien* (Ed.: R. Korthauer), Springer Berlin Heidelberg, Berlin, Heidelberg, **2013**, pp. 199–217.

[5] M. Armand, J.-M. Tarascon, *Nature* **2008**, *451*, 652.

[6] C. Vaalma, D. Buchholz, M. Weil, S. Passerini, *Nat. Rev. Mater.* **2018**, *3*, 652.

[7] T. Famprikis, P. Canepa, J. A. Dawson, M. S. Islam, C. Masquelier, *Nat. Mater.* **2019**, *18*, 1278.

[8] P. Adelhelm, P. Hartmann, C. L. Bender, M. Busche, C. Eufinger, J. Janek, *Beilstein J. Nanotechnol.* **2015**, *6*, 1016.

[9] a) D. Larcher, J.-M. Tarascon, *Nat. Chem.* **2015**, *7*, 19; b) J. L. Murray, *Bull. Alloy Phase Diagrams* **1983**, *4*, 407.

[10] I. Hasa, S. Mariyappan, D. Saurel, P. Adelhelm, A. Y. Koposov, C. Masquelier, L. Croguennec, M. Casas-Cabanas, *J. Power Sources* **2021**, *482*, 228872.

[11] P. K. Nayak, L. Yang, W. Brehm, P. Adelhelm, *Angew. Chem. Int. Ed.* **2017**.

[12] J. Janek, W. G. Zeier, *Nat. Energy* **2016**, *1*, 1167.

[13] H. Dai, Y. Chen, W. Xu, Z. Hu, J. Gu, X. Wei, F. Xie, W. Zhang, W. Wei, R. Guo et al., *Energy Technol.* **2021**, *9*, 2000682.

[14] a) Y. Zhao, K. R. Adair, X. Sun, *Energy Environ. Sci.* **2018**, *11*, 2673; b) Z. Li, P. Liu, K. Zhu, Z. Zhang, Y. Si, Y. Wang, L. Jiao, *Energy Fuels* **2021**, *35*, 9063.

[15] Y. Lu, L. Li, Q. Zhang, Z. Niu, J. Chen, *Joule* **2018**, *2*, 1747.

[16] J. A. S. Oh, L. He, B. Chua, K. Zeng, L. Lu, *Energy Storage Mater.* **2021**, *34*, 28.

[17] C. Zhao, L. Liu, X. Qi, Y. Lu, F. Wu, J. Zhao, Y. Yu, Y.-S. Hu, L. Chen, *Adv. Energy Mater.* **2018**, *8*, 1703012.

[18] B. Tang, P. W. Jaschin, X. Li, S.-H. Bo, Z. Zhou, *Mater. Today* **2020**, *41*, 200.

[19] C. Zhou, S. Bag, V. Thangadurai, *ACS Energy Lett.* **2018**, *3*, 2181.

[20] B. Lee, E. Paek, D. Mitlin, S. W. Lee, *Chem. Rev.* **2019**, *119*, 5416.

[21] W. Hou, X. Guo, X. Shen, K. Amine, H. Yu, J. Lu, *Nano Energy* **2018**, *52*, 279.

[22] Q. Ma, F. Tietz, *ChemElectroChem* **2020**, *7*, 2693.

[23] C.-H. Dustmann, *J. Power Sources* **2004**, *127*, 85.

[24] J. L. Sudworth, *J. Power Sources* **1984**, *11*, 143.

[25] "NaS-Solutions. Solutions", can be found under https://www.ngk-insulators.com/en/product/nas-solutions.html.

[26] a) K. B. Hueso, V. Palomares, M. Armand, T. Rojo, *Nano Res.* **2017**, *255*, 410; b) K. B. Hueso, M. Armand, T. Rojo, *Energy Environ. Sci.* **2013**, *6*, 734; c) B. L. Ellis, L. F. Nazar, *Curr. Opin. Solid State Mater. Sci.* **2012**, *16*, 168; d) G. Nikiforidis, M. C. M. van de Sanden, M. N. Tsampas, *RSC Adv.* **2019**, *9*, 5649; e) L. Medenbach, P. Adelhelm, in *Topics in current chemistry* (Ed.: R.-A. Eichel), Springer International Publishing, Cham, **2019**, pp. 101–125.

[27] X. Lu, J. P. Lemmon, V. L. Sprenkle, Z. Yang, *JOM* **2010**, *62*, 31.

[28] X. Lu, G. Xia, J. P. Lemmon, Z. Yang, *16th International Meeting on Lithium Batteries (IMLB)* **2010**, *195*, 2431.

[29] Y. Wang, D. Zhou, V. Palomares, D. Shanmukaraj, B. Sun, X. Tang, C. Wang, M. Armand, T. Rojo, G. Wang, *Energy Environ. Sci.* **2020**, *13*, 3848.

[30] P. Pujar, B. Gupta, P. Sengupta, D. Gupta, S. Mandal, *J. Eur. Ceram. Soc.* **2019**, *39*, 4473.

[31] D. Butts, J. Schoiber, C. Choi, G. J. Redhammer, N. Hüsing, S. Donne, B. Dunn, *Chem. Mater.* **2021**, *33*, 6136.

[32] E. Yi, E. Temeche, R. M. Laine, *J. Mater. Chem. A* **2018**, *6*, 12411.

[33] Y.-B. Niu, Y.-X. Yin, Y.-G. Guo, *Small* **2019**, *15*, 1900233.

[34] a) A. M. Skundin, T. L. Kulova, A. B. Yaroslavtsev, *Russ. J. Electrochem.* **2018**, *54*, 113; b) H. Pan, Y.-S. Hu, L. Chen, *Energy Environ. Sci.* **2013**, *6*, 2338.

[35] a) A. Mauger, C. M. Julien, *Materials (Basel)* **2020**, *13*, 3453; b) C. Delmas, D. Carlier, M. Guignard, *Adv. Energy Mater.* **2021**, *11*, 2001201; c) M. H. Han, E. Gonzalo, G. Singh, T. Rojo, *Energy Environ. Sci.* **2015**, *8*, 81; d) Y. You, A. Manthiram, *Adv. Energy Mater.* **2018**, *8*, 1701785.

[36] Z. Zhang, Y. Shao, B. Lotsch, Y.-S. Hu, H. Li, J. Janek, L. F. Nazar, C.-W. Nan, J. Maier, M. Armand et al., *Energy Environ. Sci.* **2018**, *11*, 1945.

[37] J. W. Fergus, *Solid State Ionics* **2012**, *227*, 102.

[38] G. Åvall, J. Mindemark, D. Brandell, P. Johansson, *Adv. Energy Mater.* **2018**, *8*, 1703036.

[39] J.-F. Wu, R. Zhang, Q.-F. Fu, J.-S. Zhang, X.-Y. Zhou, P. Gao, C.-H. Xu, J. Liu, X. Guo, *Adv. Funct. Mater.* **2021**, *31*, 2008165.

[40] C. Jiang, H. Li, C. Wang, *Sci. Bull.* **2017**, *62*, 1473.

[41] V. Lacivita, Y. Wang, S.-H. Bo, G. Ceder, *J. Mater. Chem. A* **2019**, *7*, 8144.

[42] a) S. Lou, F. Zhang, C. Fu, M. Chen, Y. Ma, G. Yin, J. Wang, *Adv. Mater.* **2021**, *33*, 2000721; b) R. Usiskin, J. Maier, *Adv. Energy Mater.* **2021**, *11*, 2001455.

[43] B. Dunn, H. Kamath, J.-M. Tarascon, *Science (New York, N. Y.)* **2011**, *334*, 928.

[44] A. Mauger, C. M. Julien, A. Paolella, M. Armand, K. Zaghib, *Materials (Basel)* **2019**, *12*, 3892.

[45] M. S. Whittingham, R. A. Huggins, *J. Chem. Phys.* **1971**, *54*, 414.

[46] W. Smith, M. J. Gillan, *J. Phys. Condens. Matter* **1992**, *4*, 3215.

[47] E. Lilley, J. E. Strutt, *phys. stat. sol.* **1979**, *54*, 639.

[48] W. Jabukowski, D. H. Whitmore, *J. Am. Ceram. Soc.* **1979**, *62*, 381.

[49] A. V. Virkar, G. R. Miller, R. S. Gordon, *J. Am. Ceram. Soc.* **1978**, *61*, 250.

[50] A. Hooper, *J. Phys. D* **1977**, *10*, 1487.

[51] a) J. T. Kummer, N. Weber, *A Sodium-Sulfur Secondary Battery*, SAE International, Warrendale, PA, **1967**; b) J. Coetzer, *J. Power Sources* **1986**, *18*, 377.

[52] M. V. Heinz, M.-C. Bay, U. F. Vogt, C. Battaglia, *Acta Mater.* **2021**, *213*, 116940.

[53] C. Chi, T. Katsui, T. Goto, *Ceram. Int.* **2017**, *43*, 1278.

[54] M. V. Heinz, G. Graeber, D. Landmann, C. Battaglia, *16th International Meeting on Lithium Batteries (IMLB)* **2020**, *465*, 228268.

[55] G. Graeber, D. Landmann, E. Svaluto-Ferro, F. Vagliani, D. Basso, A. Turconi, M. V. F. Heinz, C. Battaglia, *Adv. Funct. Mater.* **2021**, 2106367.

[56] N. Yabuuchi, K. Kubota, M. Dahbi, S. Komaba, *Chem. Rev.* **2014**, *114*, 11636.

[57] A. Manthiram, X. Yu, *Small* **2015**, *11*, 2108.

[58] "Conductive ceramics", can be found under http://www.ionotec.com/conductive-ceramics.html, **2013**.

[59] R. Weidl, M. Schulz, M. Hofacker, H. Dohndorf, M. Stelter, *AIP Conference Proceedings*, **2016**, *1765*, 020004.

[60] G. A. Rankin, H. E. Merwin, *J. Am. Chem. Soc.* **1916**, *38*, 568.

[61] W. L. Bragg, C. Gottfried, J. West, *Zeitschrift für Kristallographie - Crystalline Materials* **1931**, *77*.

[62] R. R. Ridgway, A. A. Klein, W. J. O'Leary, *Trans. Electrochem. Soc.* **1936**, *70*, 71.

[63] C. A. Beevers, M. A. S. Ross, *Zeitschrift für Kristallographie - Crystalline Materials* **1937**, *97*.

[64] G. Yamaguchi, K. Suzuki, *BCSJ* **1968**, *41*, 93.

[65] R. C. de Vries, W. L. Roth, *J. Am. Ceram. Soc.* **1969**, *52*, 364.

[66] J. Thèry, D. Briançon, *Sur les propriétés d'un nouvel aluminate de sodium NaAl5O8*, Paris, **1962**.

[67] M. S. Whittingham, *MRS Bull.* **2021**, *46*, 168.

[68] J. L. Sudworth, P. Barrow, W. Dong, B. Dunn, G. C. Farrington, J. O. Thomas, *MRS Bull.* **2000**, *25*, 22.

[69] a) Y.-F. Y. Yao, J. T. Kummer, *J. Inorg. Nucl. Chem.* **1967**, *29*, 2453; b) J. Felsche, *Z. Kristallogr.* **1968**, *127*, 94.

[70] R. Stevens, J. G. Binner, *J. Mater. Sci.* **1984**, *19*, 695.

[71] C. Chi, T. Katsui, T. Goto, *Ceram. Int.* **2017**, *43*, 1278.

[72] S. Barison, S. Fasolin, C. Mortalò, S. Boldrini, M. Fabrizio, *J. Euro. Ceramic Soc.* **2015**, *35*, 2099.

[73] Z. Liu, J. Chen, X. Wang, Y. Wang, D. Wang, Z. Mao, *J. Mater. Sci. Mater. Electron.* **2020**, *31*, 17670.

[74] H. A. Moghadam, M. H. Paydar, *Adv. Appl. Ceram.* **2021**, *120*, 156.

[75] S. C. Ligon, M.-C. Bay, M. V. F. Heinz, C. Battaglia, T. Graule, G. Blugan, *Materials (Basel)* **2020**, *13*, 433.

[76] M.-C. Bay, M. V. F. Heinz, R. Figi, C. Schreiner, D. Basso, N. Zanon, U. F. Vogt, C. Battaglia, *ACS Appl. Mater. Interfaces* **2019**, *2*, 687.

[77] D.-H. Lee, J.-S. Kim, Y.-H. Kim, S.-K. Lim, *ms* **2021**, *27*, 68.

[78] a) Z. Wen, J. Cao, Z. Gu, X. Xu, F. Zhang, Z. Lin, *Solid State Ionics* **2008**, *179*, 1697; b) G. E. Youngblood, A. V. Virkar, W. R. Cannon, R. S. Gordon, *Am. Ceram. Soc. Bull.* **1977**, *56*, 206.

[79] M.-C. Bay, M. V. Heinz, A. N. Danilewsky, C. Battaglia, U. F. Vogt, *Ceram. Int.* **2021**, *47*, 13402.

[80] A. I. Agustina, K. Skadell, C. L. Dirksen, M. Schulz, S. P. Kusumocahyo, *AIP Conference Proceedings* **2019**, *2175*, 20070.

[81] H. Li, H. Fan, B. Wang, C. Wang, M. Zhang, G. Chen, X. Jiang, N. Zhao, J. Lu, J. Zhang, *J. Euro. Ceramic Soc.* **2020**, *40*, 3072.

[82] K. Li, M. Ma, Y. Yang, S. Liang, X. Zhang, *Ceram. Int.* **2021**, *47*, 15017.

[83] M. Yu, S. Grasso, R. Mckinnon, T. Saunders, M. J. Reece, *Adv. Appl. Ceram.* **2017**, *116*, 24.

[84] K. Li, Y. Yang, X. Zhang, S. Liang, *J. Mater. Sci.* **2020**, *55*, 8435.

[85] S. Liang, Y. Yang, K. Li, X. Zhang, *J. Euro. Ceramic Soc.* **2020**, *40*, 4047.

[86] A. V. Virkar, J.-F. Jue, K.-Z. Fung., United States Patent 6632763.

[87] T. C. Girija, A. V. Virkar, *J. Power Sources* **2008**, *180*, 653.

[88] D.-H. Lee, S.-S. Han, Y.-H. Kim, S.-K. Lim, *Journal of Industrial and Engineering Chemistry* **2019**, *76*, 366.

[89] S. C. Ligon, G. Blugan, M.-C. Bay, C. Battaglia, M. V. Heinz, T. Graule, *Proceedings of the International Conference on Fast Ionic Transport in Solids* **2020**, *345*, 115169.

[90] C. Zhang, L. Zhang, P. Zheng, X. Zhang, *Ceram. Int.* **2020**, *46*, 12232.

[91] C. Zhang, L. Zhang, X. Zhang, P. Zheng, F. Li, *Ceram. Int.* **2020**, *46*, 3009.

[92] J. P. Boilot, A. Kahn, J. Thery, R. Collongues, J. Antoine, D. Vivien, C. Chevrette, D. Gourier, *Electrochim. Acta* **1977**, *22*, 741.

[93] J. Wu, J. Shi, Y. Hong, C. Zhu, *Mater. Res. Express* **2020**, *7*, 105502.

[94] J. Shi, Y. Hong, C. Zhu, *Crystals* **2020**, *10*, 987.

[95] C. L. Dirksen, K. Skadell, M. Schulz, M. Stelter, *Sep. Purif. Technol.* **2019**, *213*, 88.

[96] M. Ahmadi, M. Paydar, *PAC* **2020**, *14*, 56.

[97] Z. Wang, X. Feng, T. Zhang, Z. Xie, F. Song, Y. Li, *Ceram. Int.* **2020**, *46*, 24668.

[98] D.-H. Lee, D.-G. Lee, S.-K. Lim, *Ceram. Int.* **2021**, *47*, 24743.

[99] M.-C. Bay, M. V. Heinz, C. Linte, A. German, G. Blugan, C. Battaglia, U. F. Vogt, *Materials Today Communications* **2020**, *23*, 101118.

[100] H. Li, H. Fan, G. Chen, J. Zhang, B. Wang, J. Lu, X. Jiang, *J. Alloys Compd.* **2020**, *817*, 152717.

[101] H. Li, H. Fan, J. Zhang, Y. Wen, G. Chen, Y. Zhu, J. Lu, X. Jiang, B. Hu, L. Ning, *Ceram. Int.* **2019**, *45*, 6744.

[102] a) M. A. Zendejas, J. O. Thomas, *Phys. Scr.* **1993**, *47*, 440; b) G. Zhang, Z. Wen, X. Wu, J. Zhang, G. Ma, J. Jin, *J. Alloys Compd.* **2014**, *613*, 80.

[103] a) F. F. Lange, B. I. Davis, D. O. Raleigh, *J. Am. Ceram. Soc.* **1983**, *66*, C-50-C-52; b) A. I. Sitnikov, G. B. Tel'nova, A. S. Baikin, K. A. Solntsev, *Russ. Metall.* **2016**, *2016*, 307; c) S. N. Heavens, *J. Mater. Sci.* **1988**, *23*, 3515; d) L. Viswanathan, Y. Ikuma, A. V. Virkar, L. Viswanathan, Y. Ikuma, A. V. Virkar, *J. Mater. Sci.* **1983**, *18*, 109; e) D. J. Green, *J. Mater. Sci.* **1985**, *20*, 2639; f) A. Bielefeld, D. A. Weber, J. Janek, *J. Phys. Chem. C* **2019**, *123*, 1626.

[104] B. Sun, P. Xiong, U. Maitra, D. Langsdorf, K. Yan, C. Wang, J. Janek, D. Schröder, G. Wang, *Adv. Mater.* **2020**, *32*, 1903891.

[105] S. Wenzel, T. Leichtweiss, D. A. Weber, J. Sann, W. G. Zeier, J. Janek, *ACS Appl. Mater. Interfaces* **2016**, *8*, 28216.

[106] M.-C. Bay, M. Wang, R. Grissa, M. V. F. Heinz, J. Sakamoto, C. Battaglia, *Adv. Energy Mater.* **2020**, *10*, 1902899.

[107] J. L. Briant, G. C. Farrington, *J. Solid State Chem.* **1980**, *33*, 385.

[108] R. O. Ansell, *J. Mater. Sci.* **1986**, *21*, 365.

[109] F. G. Will, *J. Electrochem. Soc.* **1976**, *123*, 834.

[110] S. N. Heavens, *J. Mater. Sci.* **1982**, *17*, 965–969. https://doi.org/10.1007/BF00543514.

[111] G. Flor, A. Marini, V. Massarotti, M. Villa, *Solid State Ionics* **1981**, *2*, 195.

[112] B. Dunn, *J. Am. Ceram. Soc.* **1981**, *64*, 125.

[113] D. S. Park, R. W. Powers, M. W. Breiter, *Proceedings of the International Conference on Fast Ionic Transport in Solids* **1981**, *5*, 271.

[114] A. Sharafi, E. Kazyak, A. L. Davis, S. Yu, T. Thompson, D. J. Siegel, N. P. Dasgupta, J. Sakamoto, *Chem. Mater.* **2017**, *29*, 7961.

[115] W. Zhang, C.-D. Zhao, X.-L. Wu, *Adv. Mater. Interfaces* **2020**, *7*, 2001444.

[116] H.-J. Chang, X. Lu, J. F. Bonnett, N. L. Canfield, K. Han, M. H. Engelhard, K. Jung, V. L. Sprenkle, G. Li, *J. Mater. Chem. A* **2018**, *6*, 19703.

[117] D. Jin, S. Choi, W. Jang, A. Soon, J. Kim, H. Moon, W. Lee, Y. Lee, S. Son, Y. C. Park et al., *ACS Appl. Mater. Interfaces* **2018**, *11*, 2917.

[118] D. Landmann, G. Graeber, M. Heinz, S. Haussener, C. Battaglia, *Mater. Today* **2020**, *18*, 100515.

[119] K. Jung, H.-J. Chang, J. F. Bonnett, N. L. Canfield, V. L. Sprenkle, G. Li, *J. Power Sources* **2018**, *396*, 297.

[120] D. Spencer Jolly, Z. Ning, J. E. Darnbrough, J. Kasemchainan, G. O. Hartley, P. Adamson, D. E. J. Armstrong, J. Marrow, P. G. Bruce, *ACS Appl. Mater. Interfaces* **2020**, *12*, 678.

[121] a) J. L. Sudworth, A. R. Tilley, *The sodium sulfur battery*, Chapman and Hall, London, **1985**; b) Y. Hu, Z. Wen, X. Wu, Y. Lu, *J. Power Sources* **2013**, *240*, 786; c) K. Ahlbrecht, C. Bucharsky, M. Holzapfel, J. Tübke, M. J. Hoffmann, *Ionics* **2017**, *23*, 1319; d) D. Reed, G. Coffey, E. Mast, N. Canfield, J. Mansurov, X. Lu, V. L. Sprenkle, *J. Power Sources* **2013**, *227*, 94.

[122] M. M. Li, X. Lu, X. Zhan, M. H. Engelhard, J. F. Bonnett, E. Polikarpov, K. Jung, D. M. Reed, V. L. Sprenkle, G. Li, *Chemical communications (Cambridge, England)* **2021**, *57*, 45.

[123] K. Lu, B. Li, X. Zhan, F. Xia, O. J. Dahunsi, S. Gao, D. M. Reed, V. L. Sprenkle, G. Li, Y. Cheng, *Nano Lett.* **2020**, *20*, 6837.

[124] T. Wu, Z. Wen, C. Sun, X. Wu, S. Zhang, J. Yang, *J. Mater. Chem. A* **2018**, *6*, 12623.

[125] H. Lai, Y. Li, J. Wang, W. Li, X. Wu, Z. Wen, *Journal of Materiomics* **2021**.

[126] A. Hoppe, C. Dirksen, K. Skadell, M. Stelter, M. Schulz, S. Carstens, D. Enke, S. Koppka, *Materials (Basel)* **2021**, *14*, 854.

[127] Y. Lu, C.-Z. Zhao, H. Yuan, X.-B. Cheng, J.-Q. Huang, Q. Zhang, *Adv. Funct. Mater.* **2021**, *31*, 2009925.

[128] M. Wang, J. B. Wolfenstine, J. Sakamoto, *ADVANCES IN ELECTROCHEMICAL MATERIALSSCIENCE AND MANUFACTURING Selection of papers from the 13th ISE Topical Meeting07-10 April 2013, Pretoria, South Africa* **2019**, *296*, 842.

[129] J. Kasemchainan, S. Zekoll, D. Spencer Jolly, Z. Ning, G. O. Hartley, J. Marrow, P. G. Bruce, *Nat. Mater.* **2019**, *18*, 1105.

[130] X. Zhang, Q. J. Wang, B. Peng, Y. Wu, *ACS Appl. Mater. Interfaces* **2021**, *13*, 26533.

[131] G. J. Rees, D. Spencer Jolly, Z. Ning, T. J. Marrow, G. E. Pavlovskaya, P. G. Bruce, *Angew. Chem. Int. Ed.* **2021**, *60*, 2110.

[132] E. Kazyak, R. Garcia-Mendez, W. S. LePage, A. Sharafi, A. L. Davis, A. J. Sanchez, K.-H. Chen, C. Haslam, J. Sakamoto, N. P. Dasgupta, *Matter* **2020**, *2*, 1025.

[133] R. Haas, C. Pompe, M. Osenberg, A. Hilger, I. Manke, B. Mogwitz, U. Maitra, D. Langsdorf, D. Schröder, *Energy Technol.* **2019**, *7*, 1801146.

[134] C. D. Fincher, Y. Zhang, G. M. Pharr, M. Pharr, *ACS Appl. Mater. Interfaces* **2020**, *3*, 1759.

[135] M. J. Wang, J.-Y. Chang, J. B. Wolfenstine, J. Sakamoto, *Materialia* **2020**, *12*, 100792.

[136] R. J.-Y. Park, C. M. Eschler, C. D. Fincher, A. F. Badel, P. Guan, M. Pharr, B. W. Sheldon, W. C. Carter, V. Viswanathan, Y.-M. Chiang, *Nat. Energy* **2021**, *6*, 314.

[137] L. C. De Jonghe, L. Feldman, A. Buechele, *Proceedings of the International Conference on Fast Ionic Transport in Solids* **1981**, *5*, 267.

[138] Q. Liu, L. Zhang, H. Sun, L. Geng, Y. Li, Y. Tang, P. Jia, Z. Wang, Q. Dai, T. Shen et al., *ACS Energy Lett.* **2020**, *5*, 2546.

[139] J.-M. Doux, H. Nguyen, D. H. S. Tan, A. Banerjee, X. Wang, E. A. Wu, C. Jo, H. Yang, Y. S. Meng, *Adv. Energy Mater.* **2020**, *10*, 1903253.

[140] S. Randau, D. A. Weber, O. Kötz, R. Koerver, P. Braun, A. Weber, E. Ivers-Tiffée, T. Adermann, J. Kulisch, W. G. Zeier et al., *Nat. Energy* **2020**, *5*, 259.

[141] T. Wei, Y. Gong, X. Zhao, K. Huang, *Adv. Funct. Mater.* **2014**, *24*, 5380.

[142] K. Zhao, Y. Liu, S. Zhang, S. He, N. Zhang, J. Yang, Z. Zhan, *Electrochem. Commun.* **2016**, *69*, 59.

[143] L. Liu, X. Qi, Q. Ma, X. Rong, Y.-S. Hu, Z. Zhou, H. Li, X. Huang, L. Chen, *ACS Appl. Mater. Interfaces* **2016**, *8*, 32631.

[144] Z. Zhang, Q. Zhang, J. Shi, Y. S. Chu, X. Yu, K. Xu, M. Ge, H. Yan, W. Li, L. Gu et al., *Adv. Energy Mater.* **2017**, *7*, 1601196.

[145] a) I. Yasui, *J. Electrochem. Soc.* **1978**, *125*, 1007; b) N. Keddar, D. L. Kirk, S. G. Johnson, *Phys. Status Solidi* **1984**, *82*, 327; c) I. Yasui, T. Hattori, *Solid State Ionics* **1981**, *3–4*, 401; d) A. Imai, M. Harata, *Jpn. J. Appl. Phys.* **1972**, *11*, 180; e) S.-T. Lee, D.-H. Lee, S.-M. Lee, S.-S. Han, S.-H. Lee, S.-K. Lim, *Bull. Mater. Sci.* **2016**, *39*, 729.

[146] C. Guhl, P. Kehne, Q. Ma, F. Tietz, P. Komissinskiy, W. Jaegermann, R. Hausbrand, *ADVANCES IN ELECTROCHEMICAL MATERIALSSCIENCE AND MANUFACTURING Selection of papers from the 13th ISE Topical Meeting07-10 April 2013, Pretoria, South Africa* **2018**, *268*, 226.

[147] P. Kehne, C. Guhl, L. Alff, R. Hausbrand, P. Komissinskiy, *Proceedings of the International Conference on Fast Ionic Transport in Solids* **2019**, *341*, 115041.

[148] K. V. Kravchyk, M. Walter, M. V. Kovalenko, *Commun. Chem.* **2019**, *2*, 84.

[149] X. Chi, F. Hao, J. Zhang, X. Wu, Y. Zhang, S. Gheytani, Z. Wen, Y. Yao, *Nano Energy* **2019**, *62*, 718.

[150] D. Lei, Y.-B. He, H. Huang, Y. Yuan, G. Zhong, Q. Zhao, X. Hao, D. Zhang, C. Lai, S. Zhang et al., *Nat. Commun.* **2019**, *10*, 4244.

[151] Z. Liu, X. Wang, J. Chen, Y. Tang, Z. Mao, D. Wang, *ACS Appl. Mater. Interfaces* **2021**, *4*, 623.

[152] H. Yamauchi, J. Ikejiri, F. Sato, H. Oshita, T. Honma, T. Komatsu, *J. Am. Ceram. Soc.* **2019**, *102*, 6658.

[153] H. Yamauchi, J. Ikejiri, K. Tsunoda, A. Tanaka, F. Sato, T. Honma, T. Komatsu, *Sci. Rep.* **2020**, *10*, 9453.